LA-9095-PR
Progress Report
UC-70
Issued: January 1982

Research and Development Related to the Nevada Nuclear Waste Storage Investigations

July 1—September 30, 1981

LA--9095-PR

DE82 015029

Compiled and Edited by

W. R. Daniels
K. Wolfsberg
D. T. Vaniman
B. R. Erdal

Contributors

R. D. Aguilar
R. Anderson
W. S. Baldridge
B. P. Bayhurst
D. L. Bish
J. D. Blacic
P. L. Bussolini
F. A. Caporuscio
P. R. Carroll
J. Carter
M. R. Cisneros
B. M. Crowe
W. R. Daniels
R. R. Geoffrion
J. F. Griffith*
P. M. Halleck
P. Johnson
J. F. Kerrisk
D. M. Klassen**
S. D. Knight
F. O. Lawrence
K. Lombardo
S. Maestas
P. L. McGuire
T. J. Merson
A. J. Mitchell
D. C. Nelson
J. W. Neudecker
T. W. Newton
A. E. Ogard
P. Q. Oliver
F. V. Perry
N. A. Raybold
R. S. Rundberg
V. L. Rundberg
T. J. Shankland
W. L. Sibbitt
J. J. Simpson
K. C. Spicochi
M. L. Sykes
G. M. Thompson†
J. L. Thompson††
E. N. Treher
D. T. Vaniman
G. R. Walter†
P. L. Wanek
K. Wolfsberg

*New Mexico Institute of Mining and Technology, Socorro, NM 87801.
**Department of Chemistry, McMurry College, Abilene, TX 79605.
†Department of Hydrology and Water Resources, University of Arizona, Tucson, AZ 85721.
††Department of Chemistry, Idaho State University, Pocatello, ID 83209.

Los Alamos National Laboratory
Los Alamos, New Mexico 87545

DISCLAIMER

DISCLAIMER

RESEARCH AND DEVELOPMENT RELATED TO THE NEVADA NUCLEAR WASTE STORAGE INVESTIGATIONS

July 1 — September 30, 1981

Compiled and Edited by

W. R. Daniels, K. Wolfsberg, D. T. Vaniman, and B. R. Erdal

Contributors

R. D. Aguilar
R. Anderson
W. S. Baldridge
B. P. Bayhurst
D. L. Bish
J. D. Blacic
P. L. Bussolini
F. A. Caporuscio
P. R. Carroll
J. Carter
M. R. Cisneros
B. M. Crowe
W. R. Daniels
R. R. Geoffrion
J. F. Griffith
P. M. Halleck
P. Johnson
J. F. Kerrisk
D. M. Klassen
S. D. Knight
F. O. Lawrence
K. Lombardo
S. Maestas
P. L. McGuire
T. J. Merson
A. J. Mitchell
D. C. Nelson
J. W. Neudecker
T. W. Newton
A. E. Ogard
P. Q. Oliver
F. V. Perry
N. A. Raybold
R. S. Rundberg
V. L. Rundberg
T. J. Shankland
W. L. Sibbitt
J. J. Simpson
K. C. Spicochi
M. L. Sykes
G. M. Thompson
J. L. Thompson
E. N. Treher
D. T. Vaniman
G. R. Walter
P. L. Wanek
K. Wolfsberg

ABSTRACT

This report summarizes the contribution of the Los Alamos National Laboratory to the Nevada Nuclear Waste Storage Investigations for the fourth quarter of FY-1981.

I. INTRODUCTION

This report summarizes some of the technical contributions from the Los Alamos National Laboratory to the Nevada Nuclear Waste Storage Investigations (NNWSI) project managed by the Nevada Operations Office of the US Department of Energy during the period from July 1 through September 30, 1981. This report is not intended to be a detailed technical document but does indicate the status of some of the investigations being performed at Los Alamos.

II. WASTE PACKAGE DEVELOPMENT

A. Sorption of Anions on Possible Backfill Components (E. N. Treher and N. A. Raybold)

Investigations[1] were completed on the sorption of TcO_4^- and I^- on charcoal (Darco G-60), graphite, and on charcoal (Darco G-60) combined with tuff G1-2363, which is from the Upper Bullfrog Member and is composed primarily of quartz and feldspar with small amounts of clay and mica. Although the contacts have been completed, much of the sample counting is still in progress. The available results are given in Tables I and II. The charcoal has considerably larger sorption ratios for I^- than does the graphite although the sorption and desorption ratios increase with time for both materials. When charcoal was added in varying amounts (~0 to 50%) to tuff G1-2363, the sorption ratio increased with increasing percentage of charcoal (Table II). Two of the samples containing 10% charcoal were opened daily and stirred to ensure that oxygen was always present. Although the average R_d value was lower for these samples than for the corresponding unstirred samples, the differences, <20%, were not large.

B. Hydrothermal Alteration Experiments (E. N. Treher, M. L. Sykes, R. D. Aguilar, and N. A. Raybold)

Short-term experiments in which three tuffs from Yucca Mountain were contacted with groundwater at 152 ± 1°C were performed to study possible reactions between the solid and solution phases.[1]

Three tuff samples of different lithologies were used (Tables III and IV). Before contact with groundwater, the samples (~2-mm thick x 19-mm diam) were examined with a scanning electron microscope (SEM) to observe general surface features and mineral phases. The tuff wafers were then contacted with water

TABLE I

SORPTION OF I^- ON GRAPHITE AND CHARCOAL

Contact Time (days)		R_d (mℓ/g)	
Sorption	Desorption	Graphite	Charcoal
1		0.9	130
	1	16	290
7		1.7	350
	7	37	430
21		2.5	760
	21	250	560
42		11	6640

TABLE II

DEPENDENCE OF SORPTION OF ^{95m}Tc ON PERCENTAGE CHARCOAL IN TUFF[a]

% Charcoal	% G1-2363	Average R_d (mℓ/g)
0	100	0.17
1.0	99.0	36.9
4.3	95.7	485
10.0	90.0	1960
10.0[b]	90.0[b]	1600
50.4	49.6	35100

[a]Four-wk contact time. Technetium initially present as TcO_4^-.

[b]These samples were opened daily and stirred.

TABLE III

TUFF SAMPLES FOR INITIAL ALTERATION STUDY

Sample	Unit	Rock Type
G1-1292	Topopah Springs	vitrophyre
G1-1436	Tuffaceous Beds of Calico Hills	zeolitized nonwelded tuff
G1-2476	Bullfrog II	devitrified welded tuff

TABLE IV

MINERALOGY OF TEST SAMPLES USED IN ALTERATION STUDY

Sample	% Glass	% Clay[a]	% Zeolite[b]	% Alkali Feldspar	% SiO_2[c]
G1-1292	80-90	tr mnt	0	5-10	5-10 cr
G1-1436	0	tr i/m	65-85	5-10	10-20 Qz
					2-5 cr
G1-2476	0	tr mnt	0	30-50	25-40 Qz
		2-5 i/m			5-10 cr

[a] mnt = montmorillonite; i/m = illite/mica; tr = trace.

[b] clinoptilolite.

[c] cr = cristobalite; Qz = quartz.

from well J-13 in Teflon-lined Parr bombs. A Teflon screen was used to separate the wafer and solution, and contact between the two was made by inverting the Parr bomb during the experiment.

After a contact time of 3 wk at elevated temperature, the bombs were reinverted to separate the phases and allowed to cool. The tuff samples were again examined by SEM to determine if reaction had occurred. Sample G1-2476, containing cristobalite, alkali feldspar, and silica, showed little reaction other than some rounding of surfaces and precipitation of clays. The vitrophyre, sample G1-1292, showed greatly increased amounts of clays or other fine-grained sheet silicates, which had formed on glass edges. Globules, analyzed as pure SiO_2, also were observed. An unusual surface fracture network developed (Fig. 1), and in some cases these fractures were filled with a phase of the same composition as the glass. Sample G1-1436 showed marked dissolution of clinoptilolite crystals. In addition, the latest formed phases mordenite and cristobalite, observed by SEM before reaction, apparently dissolved. Examples of SEM photographs of sample G1-1436 before and after contact are given in Figs. 2 and 3, respectively. Figure 2 shows clumps of fresh cristobalite crystals over clinoptilolite prior to the experiment. After soaking at elevated temperature, the cristobalite is no longer present, and the clinoptilolite is distinctly etched (Fig. 3).

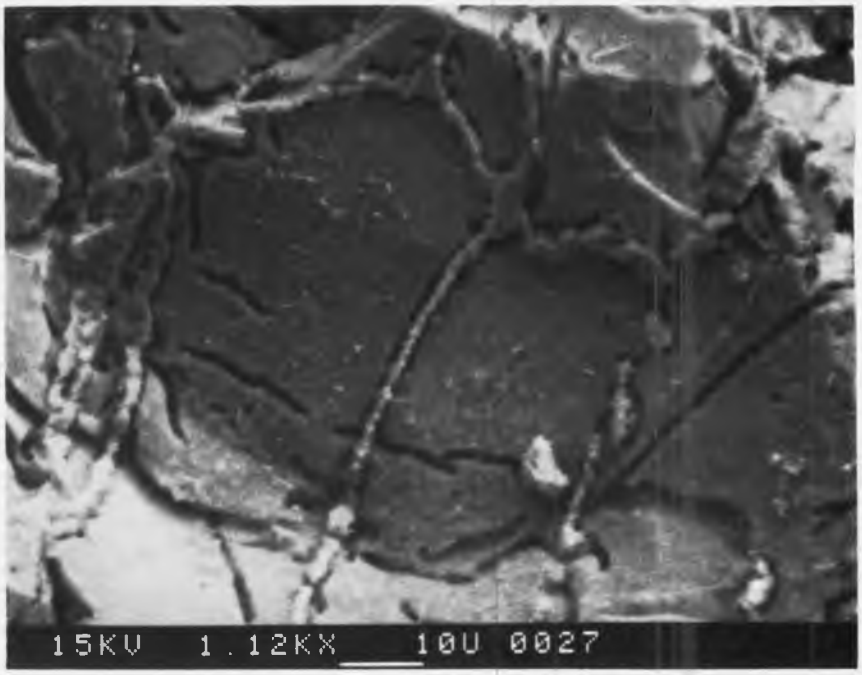

Fig. 1. SEM photograph of sample G1-1292 after contact with water from Well J-13 at 152°C for 3 wk.

Fig. 2. SEM photograph of sample G1-1436 before contact.

Fig. 3. SEM photograph of sample G1-1436 after contact.

The concentrations of the cations in the solutions after the contacts at 152°C are compared in Table V with well J-13 water treated with the same rocks at 22°C. Significant increases in the concentrations of silica, iron, potassium, and sodium and decreases in the concentration of magnesium were observed after reaction of samples G1-2476 and G1-1292 at the higher temperature. These changes represent dissolution and precipitation, respectively.

III. NUCLIDE MIGRATION EXPERIMENTS IN G TUNNEL - LABORATORY STUDIES

A. Preparation of Rock-Treated Water (A. J. Mitchell, S. D. Knight, and K. Wolfsberg)

Experimental techniques for treating ~200-ℓ quantities of groundwater with G-Tunnel tuff are being developed. Approximately 20 kg of tuff muck from a recent mining operation in the VDH-5 area was contacted with ~200 ℓ of well J-13 groundwater in a 55-gal polyethylene-lined barrel by circulating the water at a rate of ~2 ℓ/min through the tuff. The tuff was placed on an inverted polyethylene funnel in which holes had been drilled. Water was

TABLE V

COMPOSITION OF WELL J-13 GROUNDWATER

TREATED WITH USW-G1 TUFFS

	Concentration (mg/ℓ)					
	G1-2476		G1-1436		G1-1292	
Cation	22°C	150°C	22°C	150°C	22°C	150°C
Mg	1.35	0.042	0.009	0.015	1.79	0.006
Mn	0.013	0.044	0.020	0.022	0.010	0.018
Si	29.7	>60	30.8	>60	32.3	>60
Fe	0.033	0.120	0.064	0.285	0.020	0.063
Sr	0.034	0.013	0.000	0.019	0.090	0.011
Ba	0.000	0.000	0.002	0.000	0.000	0.000
V	0.010	0.000	0.019	0.000	0.000	0.021
Ti	0.004	1.02	0.000	0.549	1.72	0.000
Ca	9.50	0.657	0.176	0.031	13.1	0.534
Li	0.093	0.223	0.074	0.099	0.084	0.086
K	6.00	7.68	3.51	>10	5.02	>10
Al	0.016	0.418	0.042	0.000	0.000	3.26
Na	68.9	122 ± 4	78 ± 5	134 ± 6	57 ± 4	128 ± 2

removed from near the top of the barrel and then passed through a peristaltic pump into the funnel, where it was dispersed before circulating through the tuff. Small quantities of water were removed periodically for analysis by emission spectroscopy; results are given in Table VI. After 5 wk of contact, circulation of the water was stopped, and the water was filtered and transferred to a second barrel containing ~20 kg of fresh muck. Filtration was carried out using a Nuclepore One-Sevener filter apparatus and required three 8-h working days. We are investigating other methods for doing the filtration of large volumes of water containing finely dispersed solids. Contact with the fresh muck is proceeding to determine whether more changes in the composition of the water will occur.

TABLE VI

COMPOSITION OF G-TUNNEL TUFF-TREATED WATER

Contact Time (days)	Concentration (mg/ℓ)					
	Mg	Si	Sr	Ca	K	Na
0[a]	1.8	25	0.04	11	5	45
7	0.044	30.0	0.002	0.68	2.6	69
10	0.042	29.5	0.002	0.70	2.5	70
21	0.031	28.8	0.002	0.59	2.7	70

[a]Water from well J-13, untreated.

B. Batch Sorption Experiments (S. D. Knight and A. J. Mitchell)

Batch sorption determinations with G-Tunnel matrix tuff have been performed in a controlled atmosphere (nitrogen, ≦0.2 ppm oxygen, ≦20 ppm carbon dioxide). Sorption ratios of cesium, strontium, barium, and europium were reported earlier.[1] Table VII lists the Rd values for desorption measured for contact times of 3 and 6 wk, and Table VIII lists the average values for sorption and desorption for each time. As is expected, the equilibrium value is approached with time from low or high values depending on whether the determination is a sorption or desorption experiment, respectively. The reproducibility of duplicate determinations is poorer for this tuff than for other tuffs studied.

C. Crushed-Rock Column Experiments (E. N. Treher and N. A. Raybold)

Elution from the column of crushed fracture-fill material from G Tunnel continued.[1] After the elution of technetium,[1] the flow rate was increased from 12.9 to 131.4 m/yr because the isotopes ^{85}Sr, ^{137}Cs, and ^{133}Ba have high batch sorption ratios on this material.[1] Although no elution as such has begun, ^{133}Ba has been detected periodically in the eluate. The column of G-Tunnel tuff is showing behavior not previously seen in any column; it is gradually deteriorating and fine particles, <35 μm, are being removed with the eluate. Perhaps the ^{133}Ba seen to date has been removed on this fine material.

TABLE VII

R_d VALUES FOR DESORPTION OF CESIUM, STRONTIUM, BARIUM, AND EUROPIUM FROM G-TUNNEL MATRIX TUFF[a]

Contact Time (wk)	R_d (mℓ/g)			
	Cs	Sr	Ba	Eu
3	28 600(8.3)[b]	87 400(15.5)	22 400(9.7)	4 450(9.7)
"	20 700(7.9)	104 000(14.4)	15 000(8.9)	3 800(9.0)
6	17 900(7.8)	41 400(13.3)	4 280(8.8)	2 330(8.8)
"	7 450(7.5)	61 300(10.5)	4 580(8.8)	793(8.1)

[a]Experiments were performed under controlled-atmosphere conditions. Feed solutions were filtered through 0.05-μm Nuclepore polycarbonate membranes. Material was from hole U12G-RNM9, 10.8 to 11.9 ft in drift HF23, and the particle size was <500 μm.

[b]The values in parentheses are the standard deviations for a single measurement of the R_d values expressed in percent; they were obtained from the errors associated with the activity measurements and estimated uncertainties for the various parameters entering into the calculation. These estimated uncertainties were propagated using the rule of change of variables in a moment matrix assuming independence of the variables.

TABLE VIII

AVERAGE R_d VALUES FOR SORPTION AND DESORPTION OF STRONTIUM, CESIUM, BARIUM, AND EUROPIUM FROM G-TUNNEL MATRIX TUFF[a]

Contact Time (wk)		R_d (mℓ/g)			
Sorption	Desorption	Cs	Sr	Ba	Eu
3		15 600(400)[b]	41 000(2 000)	6 300(700)	590(40)
	6	13 000(5 000)	51 000(10 000)	4 400(200)	1 600(800)
6		12 000(1 000)	48 000(6 000)	4 600(500)	510(100)
	3	25 000(4 000)	96 000(8 000)	19 000(4 000)	4 100(300)

[a]Data from Table VII and Ref. 1.

[b]Values in parentheses are the standard deviations of the means for duplicate measurements.

D. Solid-Core Column Experiments (E. N. Treher and N. A. Raybold)

The periodic detection of ^{133}Ba in the eluate from the crushed G-Tunnel tuff column (Sec. III.C.) is not occurring in the solid-core column.[1] This core doesn't appear to be "degrading" as is the crushed-rock column, and none of the isotopes loaded (other than ^{95m}Tc and ^{131}I, described previously[1]) have been eluted.

E. Kinetic Sorption Experiments (E. N. Treher and N. A. Raybold)

Wafers (~1.0 to 1.8 g) of G-Tunnel tuff were suspended on Teflon thread and placed in well J-13 water (pretreated with the same crushed rock) containing ^{85}Sr, ^{137}Cs, ^{133}Ba, and ^{152}Eu. (Experimental details are given in Ref. 2) Some of the results were given in Refs. 1 and 2. Results to date are summarized in Table IX.

Similar measurements with ^{131}I and ^{95m}Tc were reported previously.[1] The experiments with technetium are still in progress, but the iodine experiments were terminated after 777 h of contact because so little ^{131}I remained. If all the water in the pretreated (saturated) rock had exchanged with the water that was traced with $^{131}I^-$, 1.27% of the total activity should have been detected with the wafer.[1] Data for the first 541 h were reported[1] and indicated 1.21% of the $^{131}I^-$ on the wafer. After 777 h of contact, an average of 1.51% of the ^{131}I was found on the wafers, a number ~25% higher than expected, as explained above. This observation may not actually indicate sorption, however, because at 777 h the ^{131}I had decayed to ~6% of the initial activity level and counting statistics were quite poor.

F. Fracture Flow: Radionuclide Transport in a One-Meter Fracture with One-Dimensional Flow (R. S. Rundberg)

The one-dimensional solution to the fracture-flow matrix-diffusion equation described previously[1] was used to calculate the effect of matrix diffusion, which can be expected in the G-Tunnel experiment. This, of course, is simplistic and only considers this one effect. More complex models are currently being developed that will include dispersion, porous flow in the matrix, and complex flow fields in the fracture. It is nonetheless useful to examine the results of this simple model because matrix diffusion will be a dominant mechanism affecting the transport of radionuclides by fracture flow in tuff. For several years, matrix diffusion has been considered an

TABLE IX

SUMMARY OF KINETIC SORPTION DATA FOR G-TUNNEL WAFERS

	Total Activity Sorbed[a] (%)			
Time (h)	Sr	Cs	Ba	Eu
2.78×10^{-3}	0.75	1.22	0.75	0
8.33×10^{-3}	2.40	3.92	2.15	0.44
1.67×10^{-2}	4.14	7.13	3.82	1.52
2.50×10^{-2}	6.46	11.0	5.81	2.57
3.33×10^{-2}	8.63	14.6	7.14	3.08
8.33×10^{-2}	13.3	23.0	11.5	5.16
2.50×10^{-1}	34.3	53.7	25.5	9.62
2.20×10^{1}	99.5	99.0	97.8	72.6
3.65×10^{1}	99.2	99.0	95.6	79.9
6.20×10^{1}	99.6	99.1	97.8	70.9
3.72×10^{2}	99.8	99.1	99.0	93.6
7.08×10^{2}	99.9	99.3	99.4	94.0
2.03×10^{2}	99.9	99.2	99.2	96.1
2.85×10^{3}	99.9	99.2	99.2	96.8

[a]The percent from 2.78×10^{-3} through 2.5×10^{-1} h was calculated by comparing the activity on the wafer with the total activity added. The remaining values were calculated from the activity remaining in solution compared to the original activity in solution.

important factor in element transport through fractures in crystalline rock.[3,4,5] The effect will be much more dramatic, even over relatively short distances, in tuff because the porosity is several orders of magnitude higher than granite.

The physical properties of G-Tunnel tuff have been determined in previous measurements. Table X contains a list of the nominal parameter values chosen for the purposes of these calculations. The ionic diffusion coefficient corresponds to that of strontium and is an intermediate value compared to the ionic diffusivities of most monovalent and divalent ions. Fissure apertures from 10 to 100 μm and flow velocities (U_f) from 1 m/day to 100 m/day were used in the calculations.

TABLE X

PHYSICAL PARAMETERS USED FOR THE MATRIX DIFFUSION CALCULATIONS WITH G-TUNNEL TUFF

Parameter	Symbol	value
Density	ρ	1.6 g/cm^2
Matrix porosity	ε	0.30
Constrictivity/tortuosity	α/τ^2	0.10
Ionic diffusion coefficient	D^i	7.74×10^{-10} m^2/s
Effective diffusion coefficient	D_{eff}	2.71×10^{-11} m^2/s

Figure 4 shows the activity profile for a nonsorbing tracer, $K_d' = 0$, with a flow rate of 1 m/day after 300 days. The activity has only traveled 9 cm although the water has traveled 300 m. This result is caused by the loss of tracer to the rock matrix. In Fig. 5, tracer is shown to have penetrated far beyond 1 cm. This apparent retardation occurs because at the tracer front the concentration gradient is the highest and, therefore, diffusion the fastest so that the activity in the leading edge is lost to the matrix until the concentration in the matrix builds up. These results clearly indicate that in the G-Tunnel field experiment a flow rate of 1 m/day would be too slow because the planned duration of the experiment is 30 to 60 days with both sorbing and nonsorbing tracers.

Figures 6 to 9 show similar profiles at fluid velocities of 10 m/day and 100 m/day. At 100 m/day the tracer begins to exit the 1-m fracture in 0.3 days, and at 10 m/day the tracer front ($C/C_o = 0.5$) moves 10 cm in 3 days. These velocities, therefore, show movement that is reasonable for the time scale of the experiment.

Figures 10, 11, and 12 show the surface profile for sorbing tracers with a fluid velocity of 100 m/day. Tracers having K_d values $\leq$1000 mℓ/g will move more than 10 cm in 30 days. Figure 13 shows the effect of having a 100-μm fissure aperture. A larger aperture would make it possible to use tracers with much higher K_d values or to use slower fluid velocities. However, the latter may be the only option available if equipment design limits the flow rates that can be introduced into the fracture.

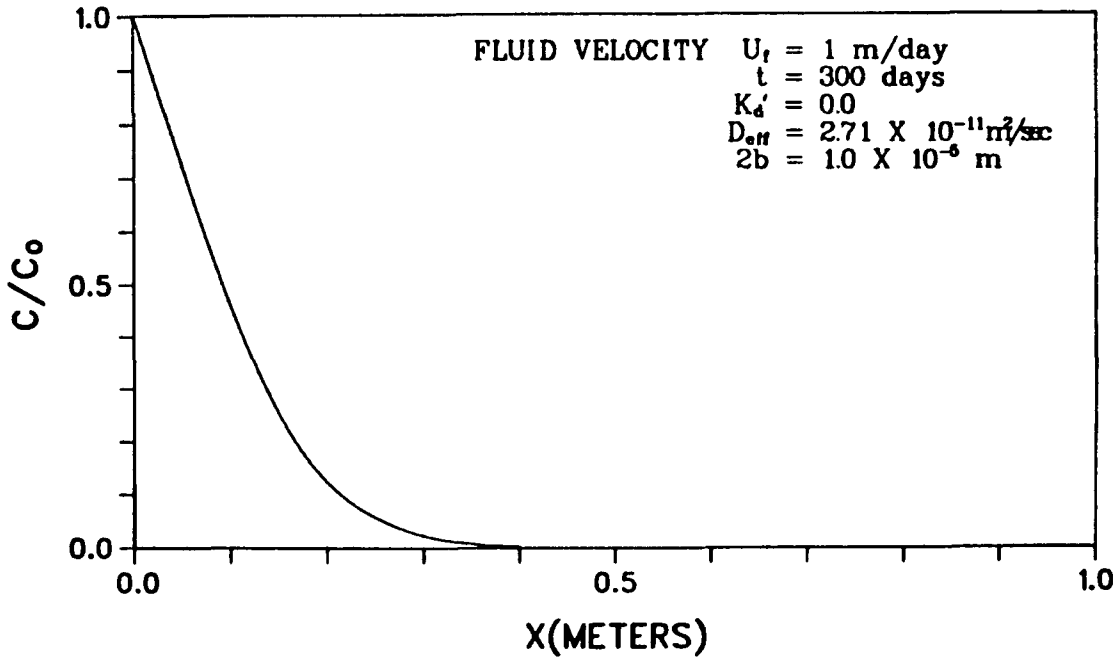

Fig. 4. Concentration profile on the fracture surface (z = 0).

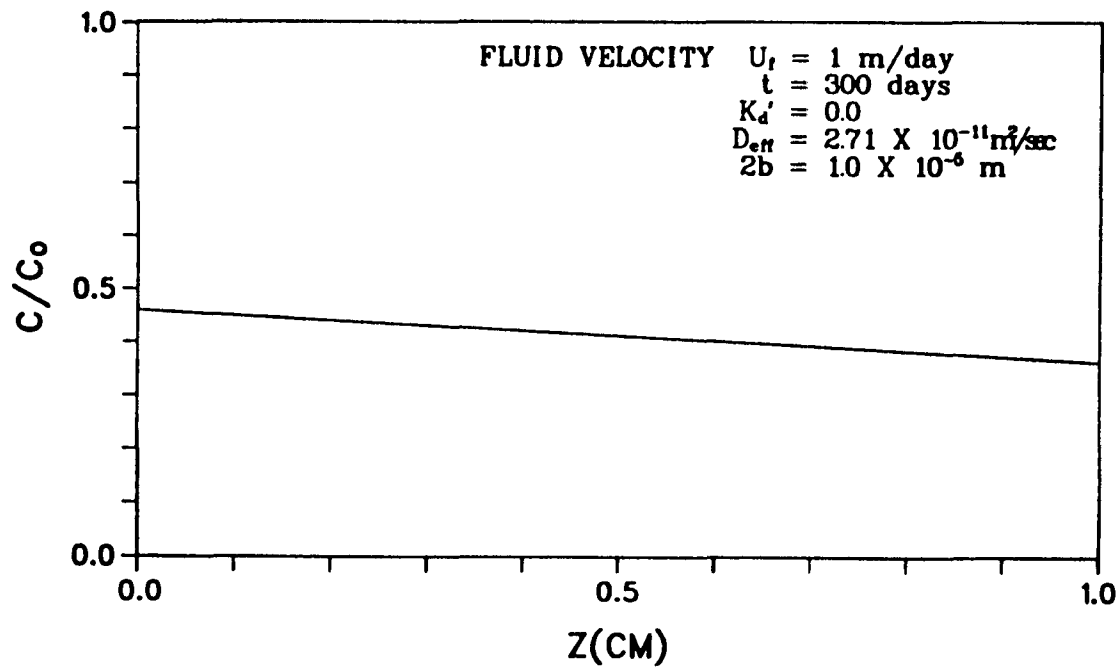

Fig. 5. Concentration profile in the rock matrix (x = 0.1 m).

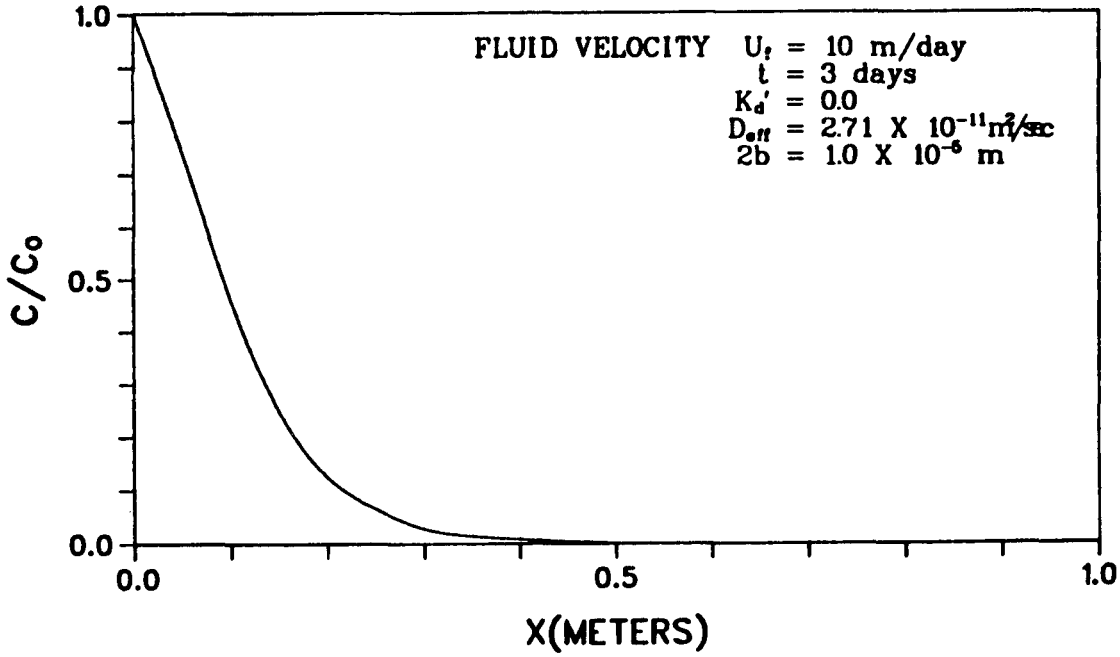

Fig. 6. Concentration profile on the fracture surface (z = 0).

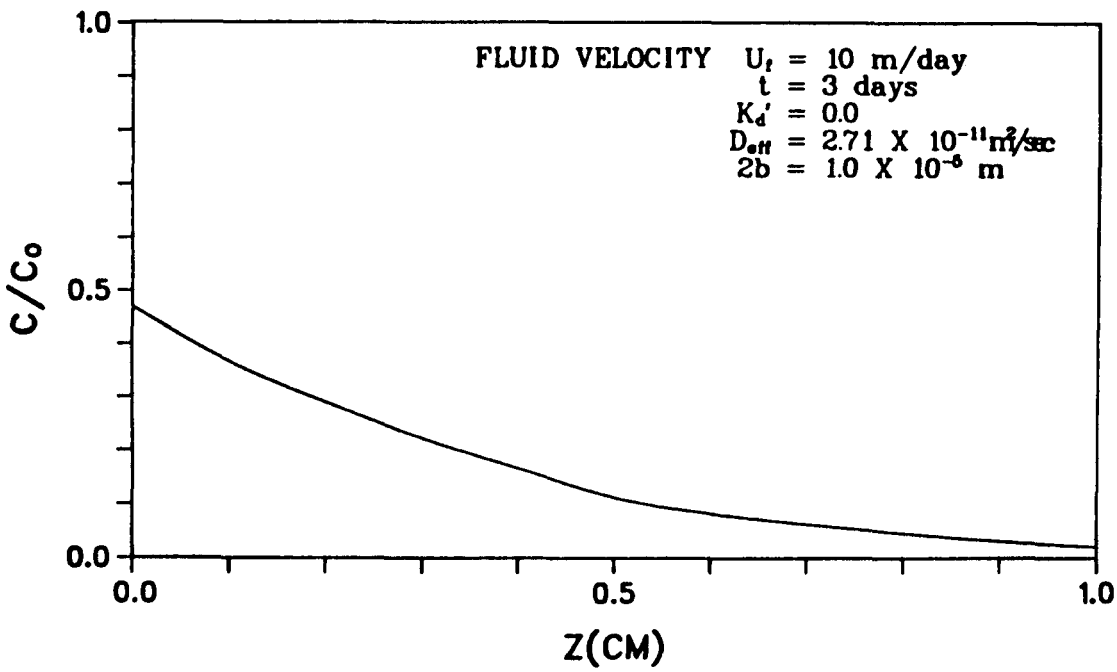

Fig. 7. Concentration profile in the rock matrix (x = 0.1 m).

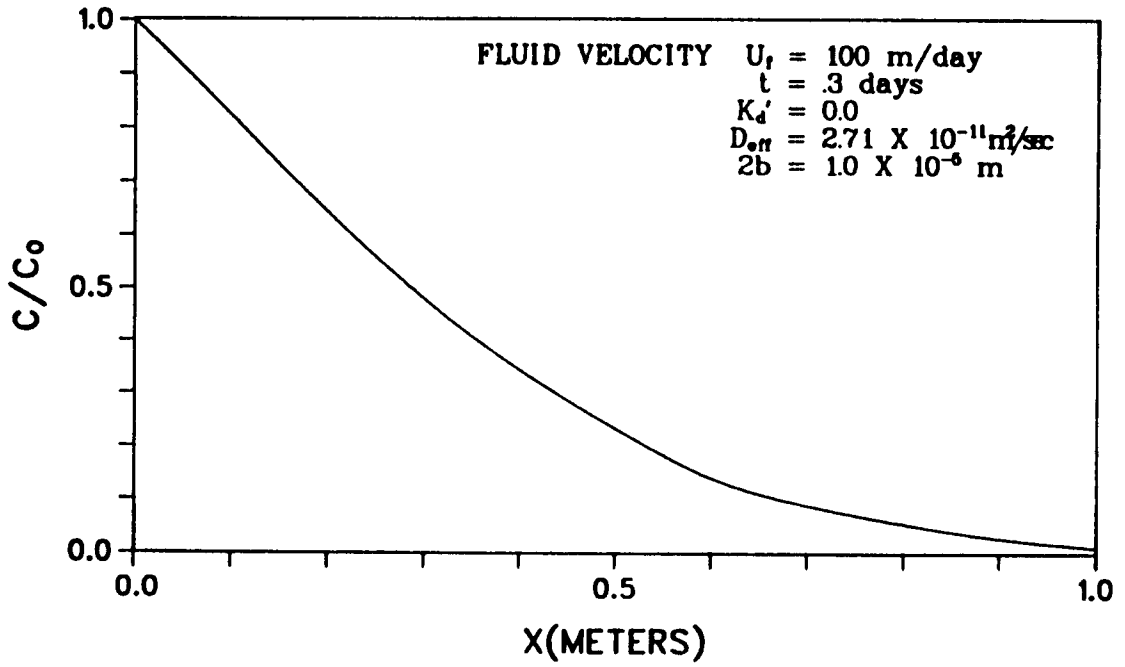

Fig. 8. Concentration profile on the fracture surface (z = 0).

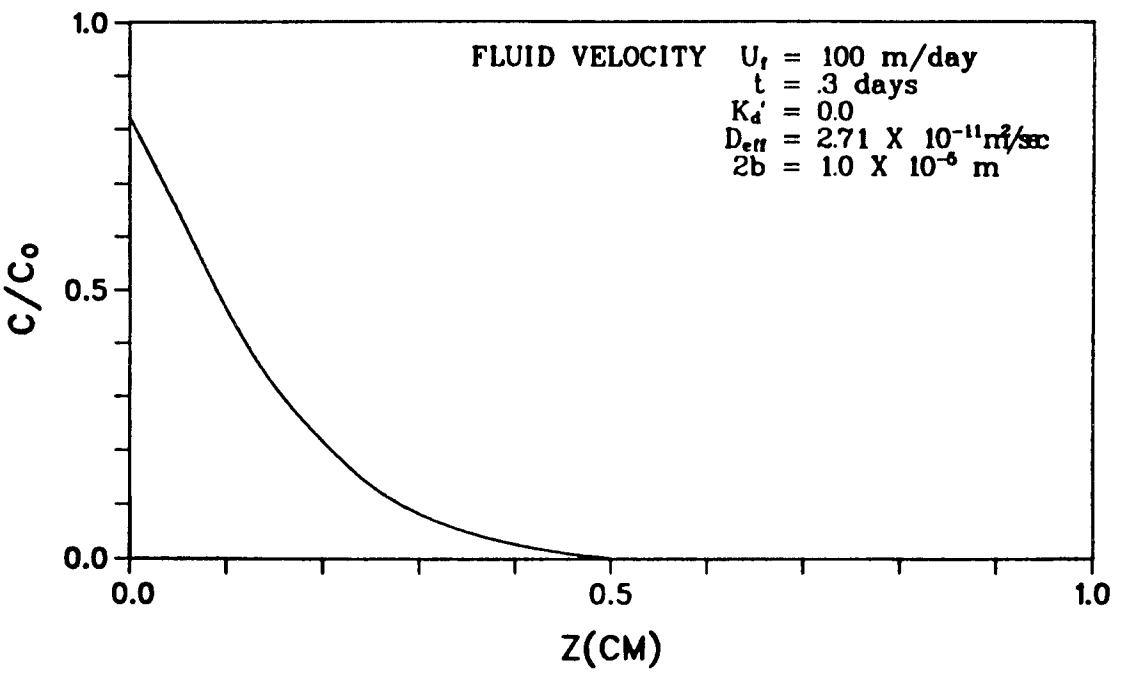

Fig. 9. Concentration profile in the rock matrix (x = 0.1 m).

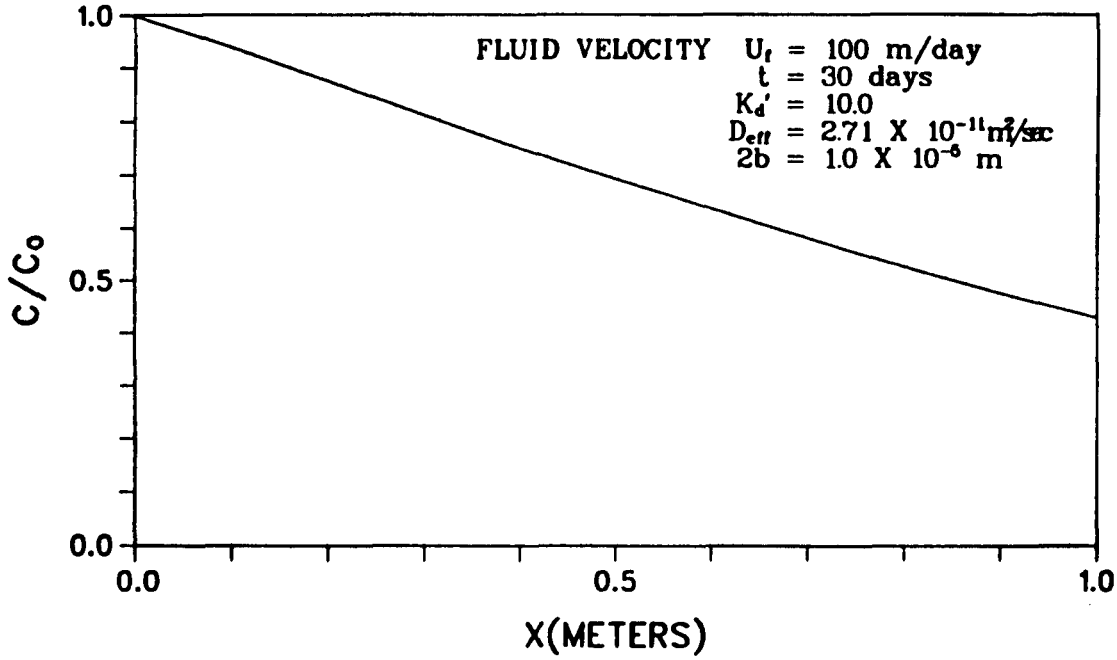

Fig. 10. Concentration profile on the fracture surface (z = 0).

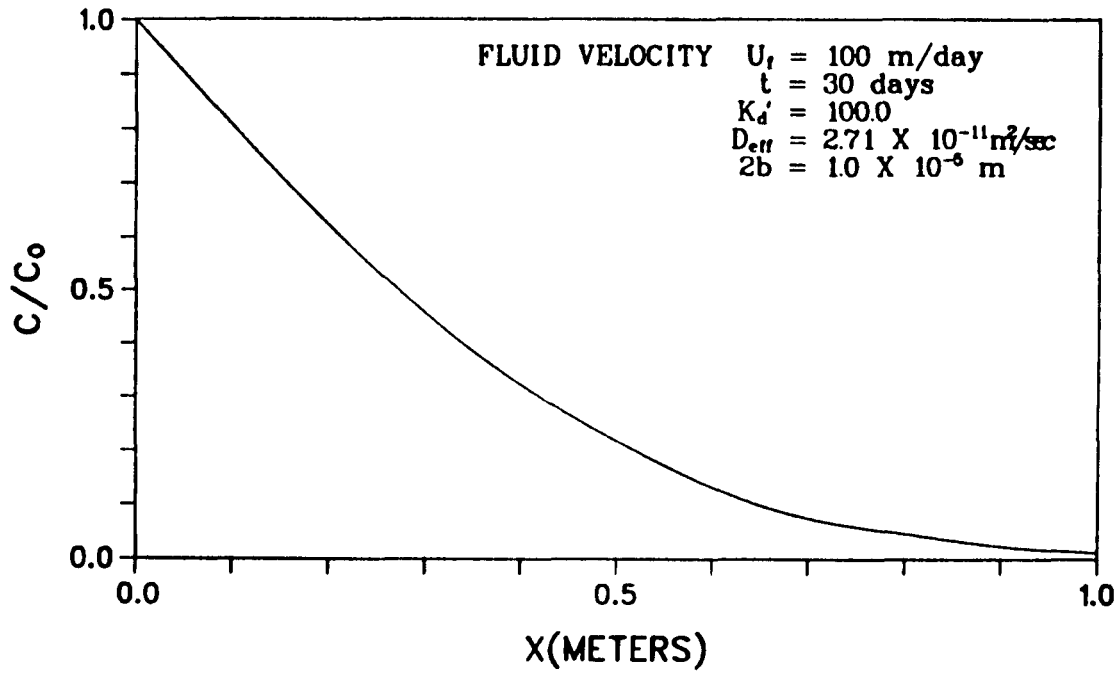

Fig. 11. Concentration profile on the fracture surface (z = 0).

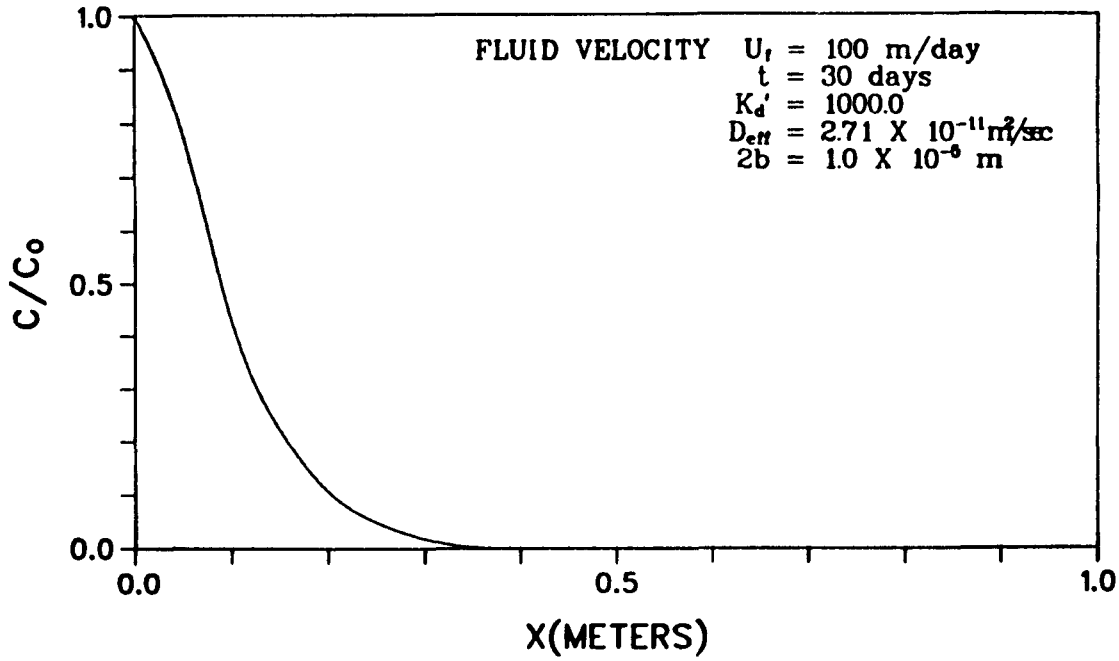

Fig. 12. Concentration profile on the fracture surface (z = 0).

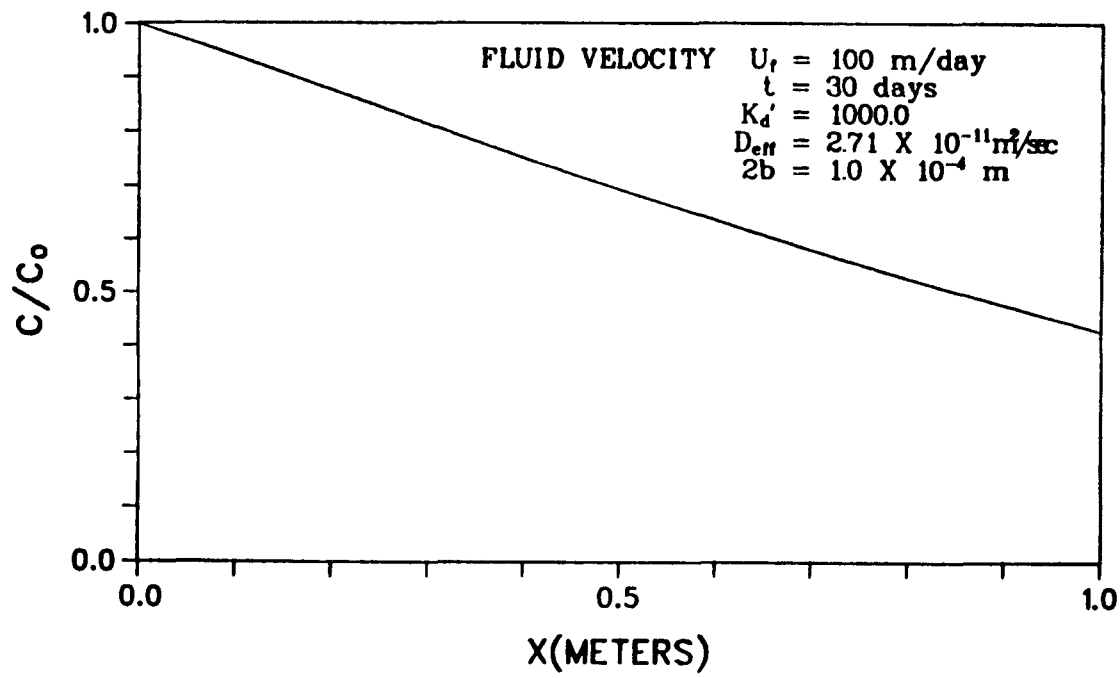

Fig. 13. Concentration profile on the fracture surface (z = 0).

Some interesting relationships are evident in these calculations: 1) To a first approximation, the distance that a given tracer travels in some fixed time interval depends on the flow rate, independent of the aperture. 2) The distance that a given tracer travels in a fixed time interval varies as the square root of the K_d value for a fixed fluid velocity.

IV. GEOCHEMISTRY OF TUFF

A. Sorption on Tuff Samples from the USW-G1 Drill Hole (S. D. Knight, A. J. Mitchell, D. L. Bish, K. Wolfsberg, and W. R. Daniels).

Several types of batch experiments were performed with tuff samples from the USW-G1 drill hole. The composition of the samples as determined by x-ray diffraction analyses is given in Table XI.

One set of experiments involved the determination of sorption ratios for a series of pulverized tuffs with two size fractions, <75 μm and 75 to 500 μm, for each tuff. Sorption times were 3 and 6 wk, and corresponding desorption times were 6 and 3 wk. Results from individual experiments are given in Table XII, and the averages of the R_d values for sorption and of the R_d values for desorption are given in Table XIII. The reason for these experiments was to further investigate the differences in R_d with particle size that were reported[1] for sample G1-1982 and that were postulated[1] to account for some of the differences in R_d values determined by batch and by crushed-rock column methods. Whereas the R_d values for the fine fractions of sample G1-1982 were generally factors of >3 higher than those for the coarser fractions, the sorption ratios for the samples in this study are much closer; on the average for the samples in Table XIII, the values for the fine fraction are only 1.4 ± 0.1 greater than those of the coarse fraction. We tentatively conclude that the differences in the behavior of the fractions from tuff G1-1982 are peculiar to the textural nature of that tuff that resulted in differences between the fine and coarse fractions. Measurements with additional samples and various fraction sizes are in progress.

In addition, Tables XII and XIII show that there are generally no large differences for R_d values for sorption and desorption, with the value for desorption generally being a little higher than that for sorption. For europium, the difference is greater, as has been observed before. The R_d values for sample G1-2476, which is not much different than the other devitrified tuffs, are significantly higher for desorption than for sorption.

TABLE XI

X-RAY DIFFRACTION ANALYSES OF TUFF SAMPLES

Sample	Particle Size (μm)	Composition (%)									
		Smectite	Illite/ Mica	Clino-ptilolite	Mordenite	Analcime	Quartz	Cristo-balite	Alkali Feldspar	Calcite	Glass
G1-1854	<75	5-10		40-60			20-40	15-30	10-30		
	75-500	5-10		30-50			5-15	15-30	20-40		
G1-1883		<2	<1				50-70	0-10	15-30		
G1-2233		<5	~5	20-40	20-40		15-30	10-20	10-20		
G1-2289			5-10	30-50	10-20		<5		30-50		
G1-2333	<75	5-10	<5				15-30	20-40	20-40		
	75-500	2-5	2-5				15-30	10-30	50-70		
G1-2410	<75	5-10	<5				20-40	5-15	30-50		
	75-500	5-10	<2				20-40	0-10	30-50		
G1-2476	<75	2-5	~2				30-50	5-15	40-60		
	75-500	<2	~2				30-50	5-15	40-60		
G1-2840	<75	2-5	2-5				40-60	0-10	30-50		
	75-500	2-5	2-5				40-60	0-10	30-50		
G1-2854	<75	<2	5-10				30-50	0-10	30-50		
	75-500	<2	5-10				30-50	0-10	30-50		
G1-2901		<2	<5				40-60	0-5	30-50	<5	

TABLE XII

SORPTION RATIOS FOR CESIUM, STRONTIUM, BARIUM, AND EUROPIUM AND USW-G1 TUFFS[a]

Sample and Fraction Size (μm)	Contact Time (wk)		R_d (mℓ/g)			
	Sorption	Desorption	Cs	Sr	Ba	Eu
G1-2333						
<75	3		1 700(2.2)[b]	220(1.2)	1 900(1.2)	2 000(4.3)
		3	1 340(7.4)	158(7.9)	1 630(7.7)	10 700(11)
	6		1 510(2.2)	216(2.1)	1 820(1.2)	3 120(4.1)
		6	1 430(7.4)	165(7.9)	1 700(7.7)	12 500(12)
75-500	3		1 200(2.1)	152(2.2)	1 200(1.1)	1 400(4.4)
		3	1 020(7.4)	112(7.9)	1 100(7.7)	6 750(9.5)
	6		1 120(2.1)	144(2.2)	1 140(1.1)	2 870(4.5)
		6	1 110(7.4)	126(7.9)	1 430(7.7)	9 830(12)
G1-2410						
<75	3		2 000(2.4)	283(2.1)		390(3.6)
		3	1 790(7.4)	244(8.0)	2 970(7.8)	5 650(9.3)
	6		2 040(2.3)	276(2.1)	3 040(1.3)	440(3.5)
		6	1 780(7.4)	251(8.0)	2 970(7.8)	10 200(11)
75-500	3		1 200(2.2)	170(2.2)		360(34)
		3	1 020(8.2)	126(8.7)	1 610(8.6)	3 330(9.4)
	6		1 300(2.1)	168(2.2)	1 780(1.1)	510(3.4)
		6	1 210(7.3)	154(9.9)	1 900(7.7)	8 730(11)
G1-2476						
<75	3		815(2.1)	49(2.7)	480(1.1)	4 600(4.4)
		3	1 840(7.4)	217(8.0)	3 490(7.8)	12 000(8.6)
	6		919(2.1)	51(2.6)	518(1.1)	5 080(3.9)
		6	1 640(7.4)	200(7.9)	3 220(7.7)	9 300(8.3)
75-500	3		660(2.1)	41(2.8)	374(1.1)	3 300(4.0)
		3	1 520(7.4)	198(8.0)	3 640(7.8)	15 200(8.9)
	6		741(2.0)	40(2.8)	396(1.1)	3 110(3.6)
		6	1 530(7.4)	206(8.0)	3 770(7.9)	15 200(8.9)

TABLE XII (cont.)

SORPTION RATIOS FOR CESIUM, STRONTIUM, BARIUM, AND EUROPIUM AND USW-G1 TUFFS[a]

Sample and Fraction Size (μm)	Contact Time (wk)		R_d (mℓ/g)			
	Sorption	Desorption	Cs	Sr	Ba	Eu
G1-2840						
<75	3		2 800(2.5)	170(2.1)	2 300(1.3)	5 000(6.2)
		3	2 510(7.4)	165(8.0)	2 840(7.8)	7 950(9.9)
	6		2 480(2.4)	171(2.1)	2 620(1.3)	6 200(6.0)
		6	2 460(7.4)	154(8.0)	2 710(7.8)	12 200(12)
75-500	3		2 400(2.4)	160(1.9)	2 000(1.3)	4 500(1.0)
		3	2 080(7.4)	135(8.0)	2 290(7.8)	7 890(9.6)
	6		2 020(2.3)	159(1.9)	2 140(1.2)	5 330(6.3)
		6	2 000(7.4)	133(8.0)	2 260(7.8)	8 030(10)
G1-2854						
<75	3		1 700(2.3)	120(2.2)	1 600(1.2)	1 100(4.2)
		3	1 350(7.4)	92(8.0)	1 610(7.8)	3 070(9.4)
	6		510(2.6)	59(2.5)	6 510(1.2)	2 560(3.4)
		6	1 860(7.4)	130(8.0)	3 700(7.8)	7 250(11)
75-500	3		1 200(2.2)	94(2.3)	950(1.1)	1 100(4.7)
		3	1 180(7.4)	97(7.9)	1 330(7.7)	5 220(10)
	6		952(2.1)	93(2.3)	1 040(1.1)	1 530(4.1)
		6	1 140(7.4)	96(7.9)	1 330(7.7)	4 780(9.4)
G1-1854						
<75	3		15 100(4.5)	71 000(12)	63 000(22)	>131 000
		3	17 900(8.4)	>37 500	252 000(12)	6 520(10)
	6		14 900(4.1)	92 000(17)	48 000(11)	>110 000
		6	13 900(8.2)	70 900(21)	145 000(10)	4 760(9.7)
75-500	3		11 400(3.9)	32 000(9.2)	34 000(9.5)	>122 000
		3	15 100(8.2)	51 100(22)	86 900(10)	4 770(9.7)
	6		10 000(3.5)	43 500(13)	34 000(8.1)	> 14 000
		6	10 900(7.9)	94 800(19)	127 000(9.9)	3 030(9.1)

[a]The numbers after the G1 designation indicate the depth of the core in feet.

[b]The values in parentheses are the standard deviations for single measurements of the R_d values expressed in percent; they were obtained from the errors associated with the activity measurements and estimated uncertainties for the various parameters entering into the calculation. These estimated uncertainties were propagated using the rule of change of variables in a moment matrix assuming independence of the variables.

TABLE XIII

AVERAGE R_d VALUES FROM TABLE XII

Sample and Fraction Size (μm)	R_d(mℓ/g)							
	Cs		Sr		Ba		Eu	
	Sorption	Desorption	Sorption	Desorption	Sorption	Desorption	Sorption	Desorption
G1-2333, <75	1 600(100)[a]	1 390(50)	218(2)	161(4)	1 860(40)	1 670(35)	2 600(600)	11 600(900)
G1-2333, 75-500	1 160(40)	1 070(50)	148(4)	119(7)	1 170(30)	1 270(170)	2 200(800)	8 300(1 500)
G1-2410, <75	2 020(20)	1 790(5)	280(4)	250(4)	3 040[b]	2 970(0)	420(30)	7 900(2 350)
G1-2410, 75-500	1 250(50)	1 120(100)	170(1)	140(15)	1 780[b]	1 750(150)	420(80)	6 000(3 000)
G1-2476, <75	870(50)	1 740(100)	50(1)	210(10)	500(20)	3 350(140)	4 800(300)	10 700(1 300)
G1-2476, 75-500	700(40)	1 530(5)	41(1)	202(4)	385(10)	3 700(65)	3 200(90)	15 200(0)
G1-2840, <75	2 640(160)	2 490(30)	170(1)	160(6)	2 500(200)	2 780(65)	5 600(600)	10 000(2 000)
G1-2840, 75-500	2 210(190)	2 040(40)	160(1)	134(1)	2 070(70)	2 280(15)	4 900(400)	7 960(70)
G1-2854, <75	1 100(600)	1 600(300)	90(30)	94(1)	4 100(2 000)	2 700(1 100)	1 800(800)	5 200(2 000)
G1-2854, 75-500	1 080(120)	1 160(20)	94(1)	97(1)	1 000(50)	1 330(0)	1 300(200)	5 000(200)
G1-1854, <75	15 000(100)	16 000(2 000)	81 000(11 000)	>70 000	56 000(8 000)	200 000(50 000)	>130 000	5 600(900)
G1-1854, 75-500	10 700(700)	13 000(2 000)	38 000(6 000)	73 000(31 000)	34 000(0)	110 000(30 000)	>120 000	3 900(900)

[a] Values in parentheses are the absolute-value standard deviations of the means.

[b] Only one measurement was available.

Sorption ratios of four tuffs for sodium (^{22}Na), manganese (^{54}Mn), selenium (^{75}Se), and tin (^{113}Sn) were determined. The results for 2- and 4-wk sorption times and the corresponding 4- and 2-wk desorption times are given in Table XIV. All experiments were done in air, except those with tuff G1-2237, which were done in the controlled atmosphere (nitrogen, $\leq$0.2 ppm oxygen, $\leq$20 ppm carbon dioxide).

Average values for sorption and desorption are given in Table XV. As is expected for sodium, the R_d values are significantly higher for the two zeolitized samples (G1-2233 and G1-2289) than for the two devitrified ones (G1-2901 and G1-1883), and the values for desorption are greater than those for sorption. Values for selenium are low, and values for desorption are somewhat higher than those for sorption.

B. Actinide Sorption Measurements Using Batch, Circulating System, and Crushed-Rock Column Methods (R. D. Aguilar, M. R. Cisneros, W. R. Daniels, F. O. Lawrence, S. Maestas, A. J. Mitchell, and P. Q. Oliver)

Experiments designed primarily to investigate the dependence of americium, plutonium, and neptunium sorption ratios on the method of determination were started during the previous quarter.[1] Batch, circulating system, and crushed-rock column methods are being studied. The original intent was to use a single traced feed solution for each nuclide and rock combination to eliminate possible variations in results with individually prepared batches of feed.[2] This was accomplished, except for the neptunium crushed-rock column experiments, which had to be repeated. Results to date for americium and neptunium sorption and desorption measurements by circulating system and batch methods are given in Tables XVI and XVII. In most cases, sorption ratios obtained by the batch method are higher than those obtained with the circulating system, which is essentially a batch contact without physical movement of the rock. The difference in R_d values may be a result of high sorption on fine particles produced by self-grinding during the batch contacts.[1] As usual,[6] R_d values for desorption tend to be greater than those for sorption. Tuff JA-37, which is high in montmorillonite, has the highest R_d values for americium. The relationship between sorptive behavior and mineralogy for these and other elements was discussed in Refs. 2, 7, and 8.

Crushed-rock column experiments with neptunium and tuffs JA-37, YM-49, and G1-1883 are in progress. Preliminary results indicate that neptunium is retarded relative to tritiated water but that sorption ratios determined by

TABLE XIV

SORPTION RATIOS FOR SODIUM, MANGANESE, SELENIUM, AND TIN FOR USW-G1 TUFFS[a]

Sample	Contact Time (wk)		R_d (mℓ/g)			
	Sorption	Desorption	Na	Mn	Se	Sn
G1-2233[b]	2		148(3)	2 450(120)	14(7)	290(90)
	4		151(7)	630(80)	14(4)	140(30)
		2	151(18)	3 120(300)	130(70)	990(330)
		4	156(9)	1 520(120)	68(4)	500(20)
G1-2901	2		2.4(1.1)	>10 000	8.8(1.7)	>10 000
	4		4.1(0.4)	>10 000	8.7(4.7)	>10 000
		2	6.7(0.2)	>10 000	81(12)	>10 000
		4	5.5(0.0)	>10 000	66(3)	>10 000
G1-2289	2		224(7)	>10 000	16(7)	840(290)
	4		230(1)	6 650(620)	11(1)	600(50)
		2	267(6)	>10 000	53(5)	1 460(80)
		4	240(13)	>10 000	27(5)	1 030(20)
G1-1883	2		2.0(1.0)	128(8)	1.5[c]	232[c]
	4		2.6(1.1)	265(127)	10(6)	460(170)
		2	2.8(1.0)	560(390)	51(21)	2 540(120)
		4	2.7(1.4)	145[c]	40(20)	2 350(600)

[a]Sorption ratios are given as the average of two measurements. Numbers in parentheses are the absolute-value standard deviations of the means. Particle size range, <500 μm.

[b]Experiments performed under controlled-atmosphere conditions.

[c]Only one measurement.

TABLE XV

AVERAGE R_d VALUES FROM TABLE XIV

	R_d (mℓ/g)[a]							
	Na		Mn		Se		Sn	
Sample	Sorption	Desorption	Sorption	Desorption	Sorption	Desorption	Sorption	Desorption
G1-2233[b]	150(4)	150(9)	1 500(500)	2 300(500)	14(3)	100(30)	210(60)	550[c](60)
G1-2901	2.9(0.6)	6.1(0.4)	>10 000	>10 000	8.8(2.0)	74(7)	>10 000	>10 000
G1-2289	230(3)	250(10)	>10 000	>10 000	14(3)	40(8)	720(140)	1 200(130)
G1-1883	2.3(0.6)	2.8(0.7)	132[c](6)	152[c](2)	6.9[c](4)	46(12)	380[c](120)	2 400(120)

[a] Sorption ratios are given as the average of four measurements, except where indicated. Numbers in parentheses are absolute-value standard deviations of the means.

[b] Experiments with tuff G1-2233 were performed under controlled-atmosphere conditions. Partical size range, <500 μm.

[c] One value was rejected.

TABLE XVI

COMPARISON OF AVERAGE AMERICIUM SORPTION RATIOS[a] FROM CIRCULATING SYSTEM AND BATCH EXPERIMENTS

Tuff Sample	R_d (mℓ/g)			
	Circulating System		Batch	
	Sorption	Desorption	Sorption	Desorption
YM-49	2 200(300)[b]	28 000(8 000)	4 300(1 400)	8 600(5 200)
JA-37	3 400(600)	110 000(40 000)	57 000(30 000)	52 000(4 800)
G1-1883	3 300(100)	36 000(7 000)	4 700(300)	7 000(900)
U12G-RNM9	3 100(700)		800(50)	

[a]Nonweighted averages of data from 3-, 6-, 9-, and 12-wk contact times, except U12G-RNM9, circulating, 3- and 6-wk, only. Rock particle size 106 to 250 μm.

[b]Values in parentheses are standard deviations of the means.

TABLE XVII

COMPARISON OF AVERAGE NEPTUNIUM SORPTION RATIOS[a] FROM CIRCULATING SYSTEM AND BATCH EXPERIMENTS

Tuff Sample	R_d (mℓ/g)	
	Circulating System	Batch
YM-49		8.5(2)[b]
JA-37		29(7)
G1-1883		6(6)
U12G-RNM9	32(3)	31(9)

[a]Nonweighted averages of sorption data from 3-, 6-, 9-, and 12-wk contact times, except U12G-RNM9, circulating, 3- and 6-wk, only. Rock particle size 106 to 250 μm.

[b]Values in parentheses are standard deviations of the means.

the column method are somewhat lower than those from the batch method, as observed for other elements.[6]

Feed solutions for actinide sorption experiments, including those of Tables XVI and XVII, have been heretofore prepared in a manner aimed at not only optimizing the actinide concentration of the feed solution, but also ensuring, as far as possible, the exclusion of any polymeric or colloidal particles.[7] The centrifugation described in Ref. 7 probably did not eliminate many particles because the feed solution was poured from the centrifugation bottle to a fresh bottle. For future experiments, the centrifugation will be eliminated, and the feed solution will be poured directly through a double filter (0.4 and 0.05 μm), thus eliminating two container changes. The method of initial removal of the activity from the tube in which it is dried has been changed to the following: first a 2- or 3-min contact with rock-treated water using a vibrator or ultrasonic cleaner; then a second 2- or 3-min contact with a fresh portion of rock-treated water, using an ultrasonic cleaner. Third and fourth contacts have been found to remove successively smaller portions of the remaining dried tracer. Ninety percent of the time, 90 to 99% of the activity that can be removed has been removed by the first two contacts.

Rock pretreatments and tracer preparations are in progress for neptunium batch sorption and desorption on a devitrified (YM-22), a zeolitized (YM-38), and a highly zeolitized (U12G-RNM9) tuff.

C. Crushed-Rock Column Studies (E. N. Treher and N. A. Raybold)

Elutions of radionuclides from ~40 columns of crushed rock have been completed or are in progress.[6,9] The majority of these columns are of tuff although granite and argillite have also been studied to provide a comparison and to determine if general conclusions can be drawn that are applicable to all three rock types. Most of the columns have been loaded with ^{85}Sr, ^{137}Cs, and ^{133}Ba and run at flow rates of 13 to 67 m/yr. When elution peaks are observed, R_d values from these experiments are typically 1 to 3 times lower than R_d values from batch measurements on the same rock for ^{85}Sr and ^{137}Cs and 2 to 5 times lower for ^{133}Ba (Ref. 8). Some of the difference between results from column and batch measurements may be caused by fine material (<35 μm) present in many batch measurements and not present in the columns.[1] The fine fractions are being examined for

possible differences in mineralogy from the coarser fractions. Other explanations for the observed differences in R_d values are being sought.

A different kind of behavior, a slow "leaking," is sometimes observed for cesium, particularly when clay, mica, or zeolites are present in more than trace amounts. For these cases, the R_d value inferred from the position at which 50% of the activity has eluted from a column is usually greater than the values from the batch measurements on the same rock. The data from batch measurements and the mineralogic descriptions of these tuffs are summarized in Table XVIII. For these samples, R_d values from desorption experiments are considerably higher than those for sorption, indicating, perhaps, that some portion of the ^{137}Cs may be irreversibly sorbed. Such an irreversible sorption might explain the slow leaking behavior observed from some columns.

Table XIX shows the results from batch measurements and also mineralogic descriptions of tuffs for which R_d values from column experiments were less than those from batch experiments. For these rocks, all tuffs, the R_d values for sorption and desorption are quite similar, and the columns gave elution peaks.

Another unusual behavior of crushed-rock columns was observed during the elution of ^{85}Sr from a column of G1-1292 tuffs (Fig. 14). This sample is a vitrophyre containing 80 to 90% glass, 5 to 10% cristobalite, 10 to 20% alkali feldspar, and a trace of montmorillonite. The broad elution curve from this column is the only such curve yet seen for ^{85}Sr. Typically, strontium elution peaks are sharp and fairly symmetrical as is shown in Fig. 15 for sample G1-1883, which contains primarily quartz and alkali feldspar. The point at which 50% of the ^{85}Sr was eluted from column G1-1292 was well past the peak (Fig. 14). In all other cases, the volume at which 50% of the ^{85}Sr eluted corresponded quite closely to the maximum of the curve.

D. Kinetic Sorption Experiments (E. N. Treher and N. A. Raybold)

A few short-term measurements of the sorption of ^{85}Sr, ^{137}Cs, and ^{133}Ba on wafers of G1-1883 and G1-1982 tuffs have been completed, and additional measurements are in progress. The wafers, ~2-mm thick by 28-mm diam, were suspended in groundwater traced with ^{85}Sr, ^{137}Cs, and ^{133}Ba. Small aliquots of each solution were removed for counting after contact times ranging from approximately 2 to 24 h. The sorption ratios calculated for each time are given in Tables XX and XXI for samples G1-1883 and G1-1982, respectively.

TABLE XVIII

DATA FOR SAMPLES FOR WHICH R_d VALUES FOR ^{137}Cs ARE GREATER FROM COLUMN MEASUREMENTS THAN FROM BATCH MEASUREMENTS

Column[a]	Description[b] (%)	Batch R_d (mℓ/g)	
		Sorption	Desorption
Granite [4]	5-15 m, <5 c, 40-60 AF, 30-50 Qz	320(30)[c]	550(40)
Argillite [2]	10-20 m, 5-10 p, 20-40 sm, 15-30 c	1 580(90)	2 680(140)
YM-38 tuff	5-15 sm, 50-70 cpt, 5-10 Qz, 5-10 AF, 10-20 cr	8 650(1 710)	13 100(0)
JA-37 tuff	20-40 sm, 5 i/m, ~5 cpt, 30-60 Qz, 15-30 AF	610(40)	850(50)

[a]The numbers in brackets indicate the number of columns completed to date.

[b]m = mica, c = chlorite, AF = alkali feldspar, Qz = quartz, p = pyrophyllite, sm = smectite, i/m = illite/mica, cpt = clinoptilolite, cr = cristobalite, tr = trace.

[c]The values quoted in parentheses are the standard deviations of the means.

TABLE XIX

DATA FOR SAMPLES FOR WHICH R_d VALUES FOR ^{137}Cs ARE LESS FROM COLUMN MEASUREMENTS THAN FROM BATCH MEASUREMENTS[a]

Column	Description (%)	Batch R_d (mℓ/g)	
		Sorption	Desorption
YM-54(3)	tr mnt, tr i/mi, 60 Qz, 30 AF	250(2)	310(20)
YM-22	<5 mnt, 40-60 Qz, 40-60 AF	340(60)	400(34)
1883A	<10 mnt, <5 m, 30-50 Qz[a], 50-70 AF	400(20)	430(3)

[a]See footnotes a, b, and c of Table XVIII; mnt = montmorillonite.

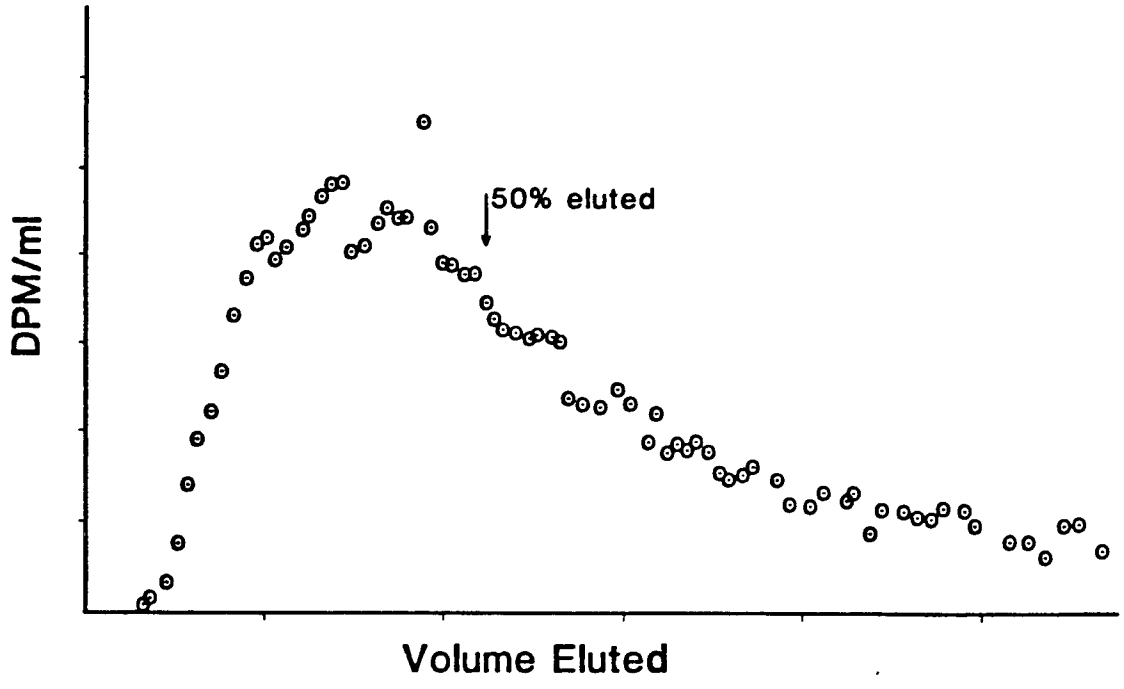

Fig. 14. Elution of ^{85}Sr from column G1-1292.

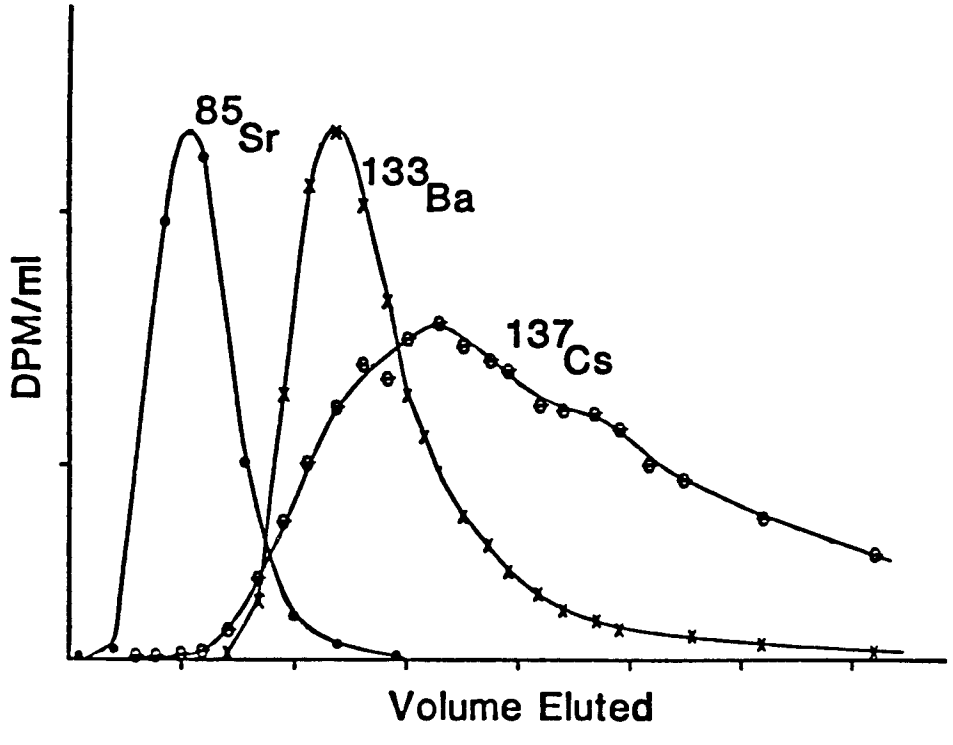

Fig. 15. Elution of nuclides from column G1-1883.

TABLE XX

SORPTION ON WAFER G1-1883

	R_d (mℓ/g)		
Time (h)	Sr	Cs	Ba
2.55	0.85	11	7.5
4.53	8.8	25	20
6.00	11	32	26
10.0	18	63	50
15.0	22	75	61
21.1	26	100	87
24.0	27	100	93

TABLE XXI

SORPTION ON WAFER G1-1982

	R_d		
Time (h)	Sr	Cs	Ba
5.0	17	65	45
7.0	30	110	78
12.0	36	180	130
16.0	45	190	170

The experiments are being continued to determine whether R_d values measured by the crushed-rock column technique are similar to those measured by this batch technique for contact times similar to the residence times in the columns.

E. Radionuclide Transport by Fracture Flow (J. L. Thompson)

Several experimental techniques related to the transport of radionuclides by fluid flow in fractured rock are under development. It is anticipated that these techniques will aid in our efforts to model flow in fractured rock. One technique involves use of a solution of an alpha-emitting radionuclide to trace the fluid flow path through a fractured rock core. The other technique

utilizes radionuclides to measure the diffusion coefficient for a dissolved species penetrating a rock matrix. The diffusion coefficient may be used to evaluate the pore constrictivity-tortuosity factor α/τ^2, which currently has to be estimated (Ref. 1 and Sec. III.K.).

Cracked cores of Climax Stock granite were utilized in experiments directed toward developing a method of tracing fluid flow paths in laboratory experiments. Small cores, 2.54 cm in diameter and 1.6 cm in length, were placed in a system in which the pressure, and hence the crack aperture, could be controlled.[8] A solution of ^{241}Am in synthetic groundwater was pumped into a crack, and the flow was stopped when the activity began to appear in the effluent. The levels of activity on the inner surfaces of the fracture indicated the path taken by the solution as it flowed through the aperture. Activity levels were measured using Kodak NTB-3 emulsion coated on a thin polymeric film sandwiched between the core faces for an appropriate exposure time. This technique seems to offer good resolution of activity levels on the rather uneven surfaces of a fracture. It does, however, require at least moderate activity levels in order to be applied in reasonable time spans. In our work, times of a few days were needed to expose the films sufficiently.

Experiments directed toward developing a method for measuring radionuclide diffusion coefficients were performed on 2.54-cm diam by 0.93-cm long cores of tuff from the USW-G1 hole. A core was sealed in a polycarbonate tube with Epoxy, and a solution of J-13 water containing a radionuclide was added to the tube. The tube and core were then immersed in a large beaker of J-13 water so that the levels of liquid inside and outside the polycarbonate tube were the same. The concentrations of radionuclide in both liquid reservoirs were measured over a period of several weeks. The first experiment was with ^{233}U solution and G1-1883 tuff. The results indicated that the ^{233}U was sorbed on the rock to a sufficient extent to prevent calculation of a diffusion coefficient. A second experiment utilizing ^{131}I as I^- ion and G1-2840 tuff gave a diffusion coefficient of the expected order of magnitude, 10^{-7} cm^2 s^{-1}. Another experiment employing tritiated water is planned for the near future.

F. Inorganic Eh Moderators and Reactions of Plutonium (T. W. Newton, D. M. Klassen, and V. L. Rundberg)

Current investigations include 1) the reaction of dilute Pu(IV) solutions to give a product that is probably polymer, 2) the reduction of Pu(V) by

$Os(acac)(bipy)_2^+$, and 3) the preparation of and the stability of additional osmium complexes for possible use as Eh buffers or moderators.

We showed previously[1] that when a 3 M acid solution of Pu(IV) is diluted to a pH of 3 and a plutonium concentration of 1.6×10^{-6} M, the amount of Pu(IV) capable of reacting with $Os(dimebipy)_3^{2+}$ decreases with time.* Possible reactions to account for this loss include

$$O_2 \text{ oxidation:} \quad 2\,H^+ + 2\,Pu(IV) + \tfrac{1}{2}O_2 = 2\,Pu(V) + H_2O \quad , \qquad (1)$$

$$\text{disproportionation:} \quad 2\,Pu(IV) = Pu(III) + Pu(V) \quad , \text{ and} \qquad (2)$$

$$\text{polymerization:} \quad n\,Pu(IV) = [Pu(IV)]n \qquad (3)$$

The effect of oxygen on the disappearance of reactive Pu(IV) was determined by adding concentrated Pu(IV) solution to either oxygen- or argon-saturated solutions containing no plutonium. The final concentrations in the diluted solutions were 4.4×10^{-6} M Pu(IV), 1×10^{-3} M $HClO_4$, and 9×10^{-3} M $LiClO_4$. After 30 min, during which the appropriate gas was passed over the surface of the solution, a 33% excess of $Os(dimebipy)_3^{2+}$ was added. Fractions of reactive Pu(IV) remaining were calculated from measured absorbance changes resulting from the oxidation of the Os(II) and found to be 0.304 ± 0.037 for the oxygen-saturated solution and 0.299 ± 0.009 for the argon-saturated solution. These data lead to the conclusion that $\lesssim$6% of the disappearance of the Pu(IV) is due to O_2 oxidation.

Disproportionation was shown to be relatively unimportant by making use of the fact that Ce(IV) in 0.5 M H_2SO_4 reacts rapidly with Pu(III) and Pu(V) but only slowly with Pu(IV). Two separate solutions, each 2×10^{-6} M in Pu(IV), 1×10^{-3} M in $HClO_4$, and 9×10^{-3} M in $LiClO_4$, were prepared from Pu(IV) in 3 M acid and were then allowed to stand for 2 min and 84 min, respectively. A sevenfold excess of Ce(IV) was next added to react with any Pu(III) and Pu(V) that might have formed; sulfuric acid was added along with the Ce(IV) so that the final solutions were 0.5 M in H_2SO_4 and 1.4×10^{-5} M in Ce(IV). Unreacted Ce(IV) was determined from the absorbance at 320 nm. The

---

*Ligands have been abbreviated as follows:

en = ethylenediamine, bipy = 2,2'-bipyridine, acac = acetylacetonate, py = pyridine, and dimebipy = 4,4'-dimethyl-2,2'-bipyridine.

two solutions showed an absorbance difference of 0.009, indicating that slightly more reducing agent was formed in the 84-min solution than in the 2-min solution. These results indicate that ~(9 ± 4)% of the Pu(IV) may have reacted to give Pu(III) and Pu(V) in the period between 2 and 84 min. Previous experiments under the same conditions showed that in the same time interval the amount of reactive Pu(IV) decreased by at least 54%. This experiment should be repeated using a more sensitive reagent, but the tentative conclusion is that most of the disappearance of reactive Pu(IV) is not due to disproportionation. This conclusion requires that the reverse of reaction (2) not be rapid in 0.5 M H_2SO_4 compared with the oxidation of Pu(III) and Pu(V) by Ce(IV). This was shown to be the case in a separate experiment.

The discussion given above makes it appear highly likely that the disappearance of reactive Pu(IV) is actually due to polymerization. This conclusion will be checked in the near future by means of filtration and sedimentation experiments.

The effect of hydrogen ion concentration on the disappearance of reactive Pu(IV) was determined in an experiment in which $OsCl(py)(bipy)_2^+$ was used as the reducing agent. The results are summarized in Table XXII. The second order rate constants found at the two hydrogen ion concentrations indicate that the empirical rate law is

$$-d[Pu(IV)]/dt = 6.2 \times 10^{-3} [Pu(IV)]^2[H^+]^{-2.2} \text{ M min}^{-1} \quad (4)$$

This rate law is written in terms of the plutonium species present in the solution in the pH range studied, 3.0 to 3.3. If the hydrolysis constants published by Baes and Mesmer[10] are accepted, the observed hydrogen ion dependence is consistent with a rate-determining step in which $Pu(OH)_3^+$ reacts with $Pu(OH)_4^0$.

A possible buffer system must react rapidly with all the plutonium species to be completely satisfactory. Our previous work[1] has shown that the reduction of Pu(VI) or Pu(IV), where no plutonium-oxygen bonds are formed or broken, is quite fast. However, further work on the Pu(IV)-Pu(V) couple is required. For this reason, we have attempted to determine the rate of reduction of Pu(V) by the strong reducing agent $Os(acac)(bipy)_2^+$. Solutions containing Pu(VI) and the Os(II) complex were mixed such that the initial concentrations of the mixtures were 2.1×10^{-5} M Pu(VI), 1.3×10^{-4} M Os(II) complex, and 2×10^{-3} M

TABLE XXII

DISAPPEARANCE[a] OF REACTIVE Pu(IV)

$(H^+) = 1.0 \times 10^{-3}$ M			$(H^+) = 5.0 \times 10^{-4}$ M		
Time (min)	Absorbance Observed	Absorbance Calculated[b]	Time (min)	Absorbance Observed	Absorbance Calculated[c]
(0.0)	1.437[d]	--	(0.0)	1.437[d]	--
1.5_3	1.480	1.476	1.1_5	1.552	1.541
12.6	1.604	1.609	1.4	1.560	1.555
			5.0_3	1.670	1.656
20.9	1.648	1.648	10.9	1.688	1.703
42.2	1.696	1.994	20.4	1.721	1.728
81.0	1.730	1.723	40.3	1.733	1.744
(∞)	1.763[d]	--	(∞)	1.763[d]	--

[a] Initial Concentrations: 3.55×10^{-6} M Pu(IV), 0.01 M (H,Li)ClO_4. Temperature: 26°C.

[b] Calculated using $k = 1.49 \times 10^4$ M^{-1} min^{-1} and the absorbance values for 0 and ∞.

[c] Same as for footnote b except $k = 1.14 \times 10^5$ M^{-1} min^{-1}.

[d] Determined in blank experiments in which the original Pu(IV) solution was added to the Os(II).

$HClO_4$. The solutions were swept free of oxygen by a stream of argon before mixing. After the solutions were mixed in the cell, it was sealed by means of a stopcock. An initial very rapid absorbance change was observed that corresponded to the reduction of Pu(VI) to Pu(V),

$$Pu(VI) + Os(II) = Pu(V) + Os(III) \qquad (5)$$

This was followed by a slow absorbance change that was monitored for a period of 122 h. The total absorbance change during this period was 3.3 times greater than the initial rapid change caused by reaction (5). This result is not consistent with the expected reaction

$$Pu(V) + 2\ Os(II) = Pu(III) + 2\ Os(III)\ , \qquad (6)$$

so some additional reaction is occurring as well. However, an upper limit of 1×10^{-6} M h^{-1} for the rate of reaction (6) can be calculated from the initial slow absorbance change. This limit corresponds to an apparent second order rate constant of 4.7×10^{2} M^{-1} h^{-1}. Further work will be required before this system is satisfactorily understood.

We prepared two osmium complexes and determined the potentials of two additional complexes. The complex $OsCl(py)(dimebipy)_2Cl$ was prepared using dimebipy rather than bipy, according to a published procedure.[11] The product was purified by the use of a Sephadex LH-20 gel-filtration column; a large amount of green material was removed from the desired product. A potentiometric titration of the purified complex indicated that the oxidation potential is ~0.41 V.

Tris(5-nitro-orthophenanthroline)osmium(II)chloride was prepared by refluxing $(NH_4)_2OsCl_6$ and the ligand in ethylene glycol using Klassen's general method.[12] Attempts to determine the standard potential were unsuccessful due to non-Nernstian behavior in the latter part of the titration. However, the data indicate that the potential is probably >1.05 V.

The potentials of two other complexes were determined. Tris[2-(2'-pyridyl)quinoline]osmium(II) perchlorate was titrated with Ce(IV) in 0.55 M H_2SO_4 and found to have a standard potential (0.104 ± 0.002) V greater than that of the tris(bipyridyl) complex. This leads to a standard potential of ~0.99 V for the complex. Tris(6-methyl-2,2'-bipyridyl)osmium(II) chloride was titrated in the same way, and the standard potential was found to be about (0.897 ± 0.002) V.

Long-term stability tests were conducted on several of the complexes dissolved in argon-swept water and sealed in Pyrex tubes. Complexes in the +3 oxidation state were prepared, using I_2 as the oxidizing agent. The spectra were determined, and the absorbance at characteristic peaks and valleys was recorded for periods of a week or more. The results are summarized in Table XXIII. It is seen that except for two of the oxidized forms, $Os(acac)(bipy)_2Cl_2$ and $OsCl(py)(dimebipy)_2Cl_2$, the spectral changes are quite small.

G. Sulfide Electrode Studies (A. E. Ogard and J. F. Griffith)

The sulfide-ion electrode contains a silver sulfide membrane. The voltage across this membrane is a function of the Ag^+ concentration and can be expressed in terms of the S^{2-} concentration by use of the solubility product of Ag_2S. The potential of the electrode can then be expressed by the Nernst equation

TABLE XXIII

STABILITY OF VARIOUS OSMIUM COMPLEXES IN WATER AT ROOM TEMPERATURE

Complex	Observation Period (days)	Spectral Changes (% day^{-1})
$Os(en)(bipy)_2I_2$	73	+0.01 to +0.03
$Os(en)(bipy)_2I_3$	11	0 to -0.23
$Os(acac)(bipy)_2Cl$	20	0 to -0.05
$Os(acac)(bipy)_2Cl_2$	12	-1 to -4
$OsCl(py)(dimebipy)_2Cl$	9	-0.15 to -0.42
$OsCl(py)(dimebipy)_2Cl_2$	9	-0.88 to -1.6

$E_{S^{2-}} = (E^{\circ}_{S^{2-}}) - \frac{RT}{2F} \ln(S^{2-})$. A plot of measured $E_{S^{2-}}$ vs log (S^{2-}) should be a straight line of slope -29.58 mV for each decade change of concentration. Figure 16 shows our results for the change in the sulfide-electrode potential as the S^{2-} concentration is varied in the range of 4×10^{-3} M to 4×10^{-9} M. The four sets of experiments were either done at pH 8 or the measurements corrected to pH 8. The lower limit of accurate detection of S^{2-} from this graph is $\sim 4 \times 10^{-5}$ M (±20%). However, the sulfide electrode is qualitatively useful to concentrations as low as 10^{-9} M.

Figure 17 shows the effect of ionic strength on the electrode potential of S^{2-} solutions. Sulfide solutions were prepared over the concentration range of 4×10^{-3} M to 4×10^{-9} M, adjusted to pH 8 ± 1, and the S^{2-} potentials were measured. Sufficient KCl was then added to each solution to make it 0.1 M in KCl, and the S^{2-} potentials of the solutions were again measured with the sulfide-ion electrode. From Fig. 17 it can be seen that at S^{2-} concentrations below 4×10^{-6} M the ionic strength of the solution has a large effect.

Complexes of H^+ and S^{2-} form as the activity of a solution is increased. At pH 11 the major species in solution is S^{2-}, whereas at pH 7 and pH 4, the major species are HS^- and H_2S, respectively. Because the sulfide-ion electrode responds only to S^{2-}, all manufacturers have recommended that the pH of a solution be adjusted to pH 11 before measurement. Boulègue[13] has shown that

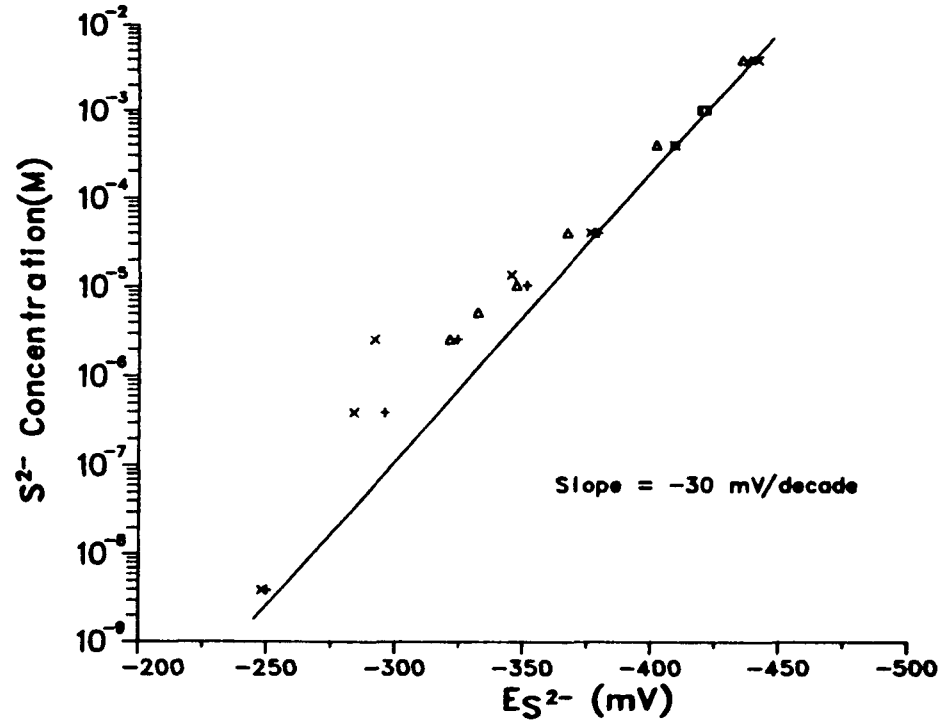

Fig. 16. Variation of sulfide-electrode potential with sulfide concentration.

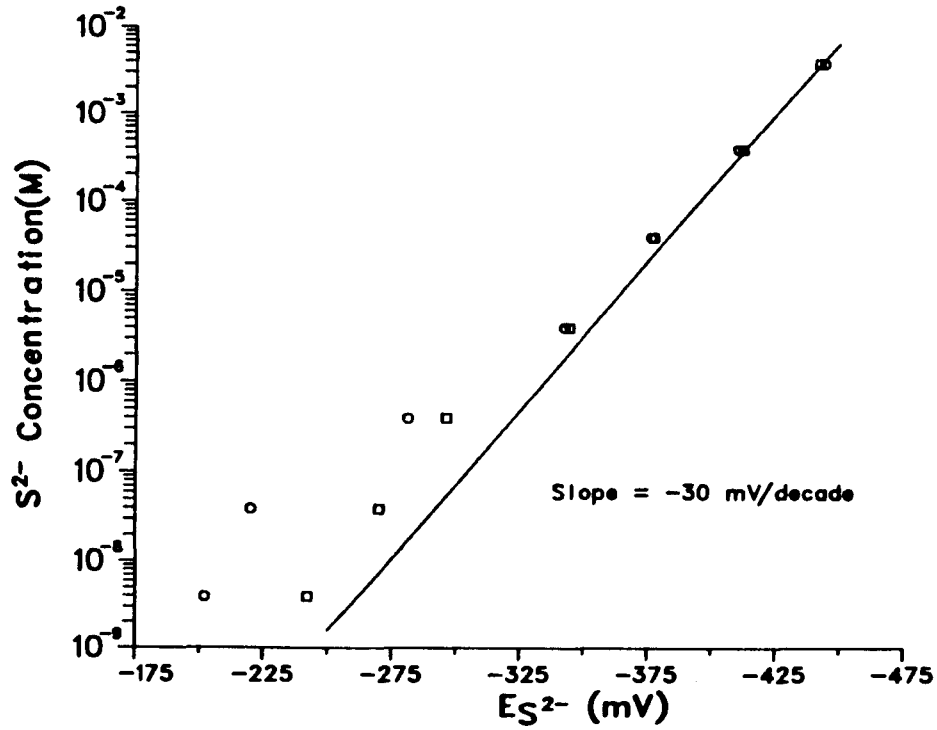

Fig. 17. Effect of ionic strength on sulfide-electrode potentials.

this is not necessary. The S^{2-} concentration and electrode potential can be calculated for any pH and total H_2S and used to form calibration curves as $E_{S^{2-}}$ vs pH. We have also shown (Fig. 18) that the electrode-measured S^{2-} potentials agree quite well with the calculated values. Eight sets of experiments, in which the S^{2-} concentration was 10^{-3} M, are shown on the graph. Also included are calculated $E_{S^{2-}}$ vs pH lines.

The manufacturers also recommend using an antioxidant such as ascorbic acid in the solution so that the S^{2-} will not oxidize. The reaction of S^{2-} with air is reasonably slow, and we found (Fig. 18) that the antioxidant is not necessary if the measurements are carried out within a reasonable time after sampling, such as a few hours. At most, the measured potential increases by 20 mV in the presence of air in the solution.

A platinum Eh electrode can be used in a sulfide system to measure the potential of the half-cell $S^{2-} = S + 2e^-$. By the Nernst equation $Eh = E° - 0.0295 \log (S^{2-})$. Combining this equation with the equation for the potential of a sulfide-ion electrode, one gets $Eh = E_{S^{2-}} + (E° - E°_{S^{2-}})$. $(E° - E°_{S^{2-}})$ was estimated by Boulègue and Michard[14] from thermodynamic data to be 180 mV. Therefore, $Eh = (E_{S^{2-}}) + 180$ mV. This equation is plotted in Fig. 19, together with our measurements (shown as x and +) of Eh and $E_{S^{2-}}$, carried out in the oxygen-free nitrogen atmosphere of a Vacuum Atmosphere glove box. In an oxygen-free atmosphere, the Eh - $E_{S^{2-}}$ relationship is very good.

In addition, we have plotted Eh and $E_{S^{2-}}$ measurements for solutions of constant S^{2-} concentration but with different oxygen contents. The vertical lines connect experiments of equal pH and supposedly the same Eh and $E_{S^{2-}}$. The uppermost measurements on each line represent solutions either in air or in a poor glove box that had air leaks. The middle points represent these same solutions after the addition of ascorbic acid to remove the oxygen in the solution. Three conclusions can be drawn from this figure. 1) Eh electrode measurements are influenced by oxygen contamination, even in a sulfide environment. 2) The sulfide electrode is not affected to a large extent by the oxygen contamination. 3) Ascorbic acid either does not eliminate all the oxygen in a solution or does not clean the Eh electrode enough to give a reading that represents the absence of oxygen.

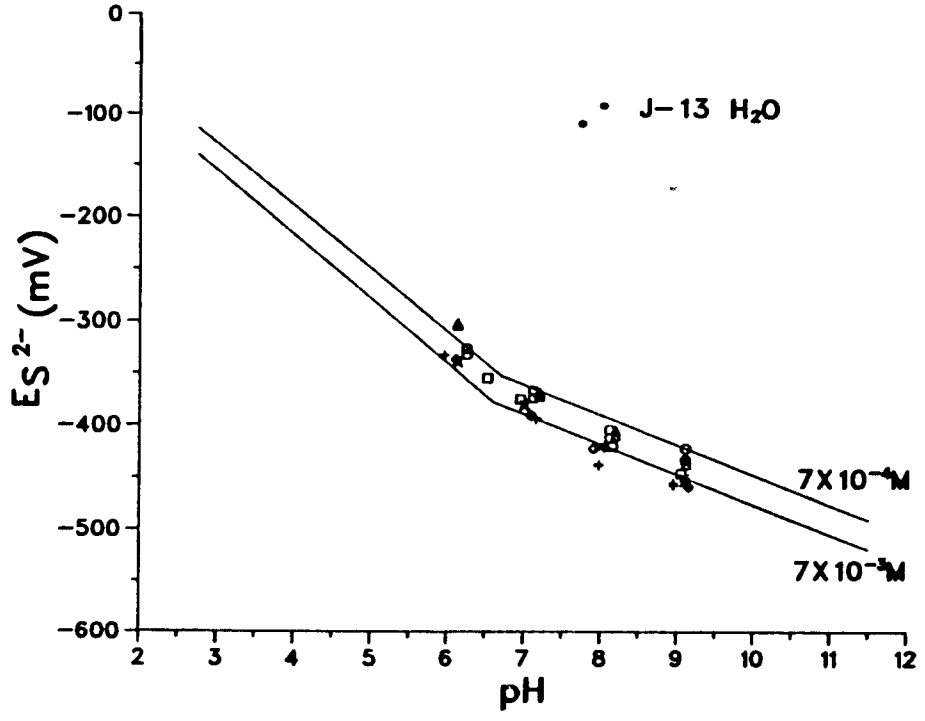

Fig. 18. Variation of sulfide-electrode potential with pH.

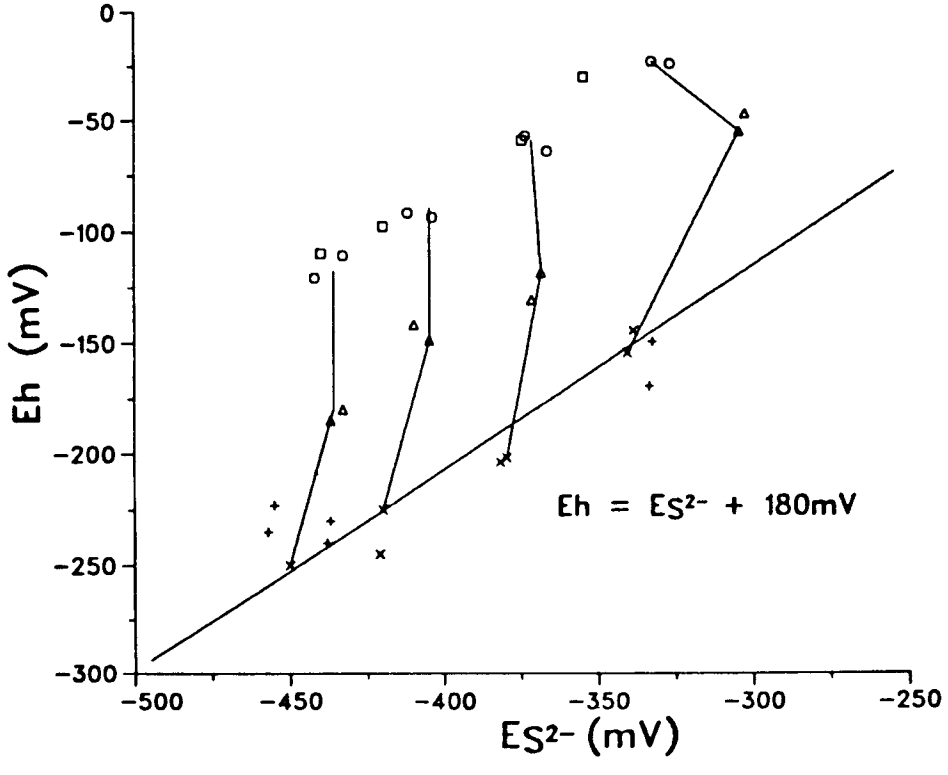

Fig. 19. Relationship of Eh and $E_{S^{2-}}$ for sulfide solutions with varying oxygen contents.

It would be interesting to pursue this study further to test whether the divergence of the Eh measurement from the Eh = ($E_{S^{2-}}$) + 180 mV relationship can be used as a measure of the oxygen content of the solution.

The Eh and $E_{S^{2-}}$ values were measured for J-13 water inside the inert-atmosphere glove box. This water had been kept sealed and inside the glove box most of the time since being collected at the wellhead. An Eh of +100 mV vs the H_2 electrode and an $E_{S^{2-}}$ of -100 mV were measured. These results agree quite well with the expression Eh = ($E_{S^{2-}}$) + 180 mV. However, it is still uncertain what the measurements really mean because the S^{2-} concentration is below the limits of accurate detection (Figs. 16 and 18), and there are no known redox couples of sufficient concentration in J-13 water to give a meaningful Eh measurement.

H. Determination of Fe(II) in Silicate Rock (B. P. Bayhurst)

The procedure for using ^{131}I in the ICl reagent for Fe (II) has not produced as accurate results as expected.[1] The results for the standards usually have a standard deviation of about 3%. Reasonable results have been obtained analyzing some US Geological Survey (USGS) standard rock; however, standard USGS-G1, a granite that does not have a homogeneous color, gives very diverse results. Part of the difficulty in the procedure probably arises from doing severalwashes to completely remove the original ^{131}ICl added, while retaining 100% of the $^{131}I_2$ in the organic phase. A container leakage problem has apparently been solved by the use of Parafilm M Laboratory Film around the threads of the closure.

Spectrophotometer scans will be made at various wavelengths to identify highly absorbing spectral regions from I_2 in various organic solvents. A spectrophotometric method would eliminate numerous manipulation problems, but would still require the removal of fluoride used in the rock dissolution.

G-Tunnel core U12G-RNM9 was analyzed twice, and the Fe(II) was found to be below the limit of detection (~0.1%).

I. Determination of Anions in Groundwater (P. L. Wanek)

Development of methods for the determination of anion concentrations in groundwater has continued.[1] New columns were installed on the ion chromatograph, which improved the reproducibility of standard anion analysis and which greatly reduced analysis time.

A method was devised to keep atmospheric perturbation of samples to a minimum, particularly for analysis of those samples that had been processed in a controlled atmosphere (nitrogen, <0.2 ppm oxygen, <20 ppm carbon dioxide). Samples were stored in a Vacutainer evacuated blood-collection tube (Becton-Dickinson, 165 x 16 mm, silicon coated, plain with no anticoagulant) until analysis. This method allowed direct transfer through a 21-gauge needle from the Vacutainer tube to a syringe and then, with needle removed, from the syringe to the chromatograph injection port without significant exposure of the sample to air. For filling tubes with samples in the controlled atmosphere, the caps were removed from the tubes, the samples were poured into the tubes in the nitrogen atmosphere, the caps were replaced, and the tubes were removed from the controlled environment. Measurement of pH with little exposure to air could be made by removing the cap and inserting a combination pH electrode (12 mm o.d.) into the tube.

Carbonate and anions of strong acids (F^-, Cl^-, NO_3^-, PO_4^{-3}, and SO_4^{-2}) could not be determined simultaneously on the ion chromatograph with a single injection, as was originally hoped, because of peak interference problems between carbonate and chloride. However, they could be run simultaneously by injecting each of the two chromatograph systems (carbonate and standard anions) separately. The Vacutainer apparently preserved samples well enough to obtain reproducible results for replicate injections, at least when the replicates were run within a few hours of one another.

Data for analyses of several waters are shown in Table XXIV. Values for anions in air-exposed samples are fairly comparable to available data from the USGS for those samples.[6,7,15] In addition, there is little systematic variation between air-exposed and controlled-atmosphere samples in the values for fluoride, chloride, and sulfate ions. Data from the USGS for aerobic/anaerobic paired analyses on water samples that had been treated with YM-38 and YM-54 tuffs support this observation.[6] The limited data available from the USGS for carbonate and nitrate concentrations tend to be inconsistent with our results, particularly for the waters that were in the controlled atmosphere.

Some of the discrepancies in bicarbonate concentrations can perhaps be attributed to differences in the duration of exposure of the solutions to the controlled atmosphere, the sampling procedures, the method of analysis, and variations in pH and amount of free carbon dioxide in the sample at the time of measurement. The analysis of water samples contacted by tuffs YM-38 and

TABLE XXIV

CONCENTRATIONS OF ANIONS IN WATER

Sample[a]	Concentration (mg/ℓ)				
	Carbonate Species	Fluoride	Chloride	Nitrate	Sulfate
Well J-13 (open)	130(124-130)[b]	3.0(1.7-2.0)	8.8(7.5-8.4)	9.4(5.6)	25(20-25)
Well J-13 (CA)[c]	100(-)[d]	2.4(-)	7.3(-)	n.d.[e](-)	25(-)
YM-38 (open)	100(110)	2.2(2.5)	6.9(7.5)	7.4(-)	18.9(26)
YM-38 (CA)	52(100)	3.2(2.6)	9.3(6.6)	n.d.(-)	25(23)
YM-54 (open)	- (110)	- (2.6)	- (6.8)	- (-)	- (24)
YM-54 (CA)	49(100)	2.3(2.5)	8.3(6.5)	n.d.(-)	22(23)
YM-22 (open)	- (-)	- (2.6)	- (6.8)	- (-)	- (24)
YM-22 (CA)	74(-)	2.4(-)	7.6(-)	n.d.(-)	20(-)

[a]Water from well J-13 was analyzed before and after contact with the indicated tuffs and filtration.

[b]Numbers in parentheses are values determined by the USGS.[6,7,15]

[c]CA = controlled atmosphere.

[d]A dash indicates no data available.

[e]n.d. = not detected.

YM-54 was performed by the USGS in September 1979, while the Los Alamos samples were not removed from the controlled atmosphere and analyzed until July 1981. The relationship between bicarbonate species measured by the USGS method of titration of alkalinity and carbonate species measured by ion chromatography is not clear. An understanding of possible factors influencing determinations of carbonate species by ion chromatography, including stability of the standards and samples when exposed to the atmosphere, subsequent change in pH, and instrumental parameters of sensitivity and linearity of response to changes in carbonate concentration, need to be investigated further.

The apparent disappearance of nitrate and possible appearance of nitrite species in the water that had been contacted with tuff YM-22 and maintained in a controlled atmosphere could be made more meaningful by adjusting instrumental parameters to provide minimum detection limits for nitrite and nitrate.

J. Theoretical and Experimental Determination of Matrix Diffusion and Related Solute Transport Properties of Fractured Tuffs from the Nevada Test Site

(G. R. Walter and G. M. Thompson)

1. Introduction. Last quarter,[1] a mercury infusion porosimeter was constructed and pore-size distribution measurements were made on bedded tuff sample G1-2290 from Yucca Mountain and sample HF23 taken from the wall of the HF23 drift near the RNM9 hole of G Tunnel. The theoretical median pore diameter of sample G1-2290 was found to be 3.9×10^{-5} cm, and the pore-size distribution was approximately log-normal between 10^{-2} cm and 10^{-5} cm. The median pore diameter of sample U12G-RNM9 was $<10^{-5}$ cm but may be approximately 3×10^{-6} cm.

Diffusion experiments using diaphragm diffusion cells were performed on tuff sample U12G-RNM9, 0.1 to 1.0 ft, taken near the fracture, and sample G1-2290. For NaBr, the respective diffusion coefficients were 7.6×10^{-7} and 4.0×10^{-7} cm^2/s. The free aqueous diffusion coefficient for NaBr is 1.7×10^{-5} cm^2/s. After correcting the sample G1-2290 value for porosity and tortuosity, the diffusion coefficient is still 0.2 of the free aqueous value.

Characterization of the chemical and physical properties affecting diffusion of the fluorobenzoate tracers is still in progress. We have not been able to duplicate published values of the acid dissociation constants for these tracers, perhaps because of residual impurities in the tracers. Further attempts to measure these values are in progress.

No evidence of complexation or ion pairing between the fluorobenzoate anions and transition metals has been observed. The fluorobenzoates do form insoluble salts with Cu^{+2}, Pb^{+2}, and Ag^{+} ions.

The limiting ion conductances of the fluorobenzoates have been measured and their diffusion coefficients at infinite dilution computed from these values. These diffusion coefficients range from 0.72×10^{-5} cm^2/s for pentafluorobenzoate to 0.93×10^{-5} cm^2/s for p-fluorobenzoate. Direct determination of these diffusion coefficients will be started soon using the diaphragm diffusion cells.

The partial differential equations governing isothermal, multicomponent transport through a single fracture in porous rock have been formulated in a form suitable for solution by the integrated finite-difference technique.

2. Properties of Tuff. Work during the first quarter of the project consisted of designing and constructing experiments and apparatus for measuring properties of tuff that will affect diffusion.

a. Porosity. A mercury infusion porosimeter was constructed for porosity and pore size distribution studies. A schematic drawing of the mercury infusion apparatus is shown in Fig. 20. The mercury porosimeter was constructed by modifying an existing Ruska mercury pump and pycnometer for use as a porosimeter by adding a polycarbonate, mercury-level-observation tube to the top of the pycnometer and the necessary pressure and vacuum regulation and measurement system. System pressures are measured using a Setra 0 to 2000 psig pressure transducer and digital read-out. The transducer also measures partial vacuums. The porosimeter is now capable of operating from pressures ranging from ~13 Pa (1 mm Hg) to 1.4×10^{6} Pa (2000 psia). The porosimeter is thus capable of measuring pore-size distributions for pores with theoretical diameters between 0.1 cm and 10^{-5} cm. The porosimeter meets or exceeds the specifications of commercially available porosimeters and has a total system expansion correction of <0.4 cm^3 at maximum pressure.

Initially, daily temperature fluctuations of several degrees Celsius in our laboratory caused problems in making accurate volume measurements. This problem has been partially corrected by repairs made to the laboratory cooling system and application of an ambient room temperature correction factor to the raw volume data. To more accurately measure the working temperature in the mercury reservoir, we plan to place a thermistor temperature probe in the mercury reservoir as soon as the necessary equipment is received from the vendor.

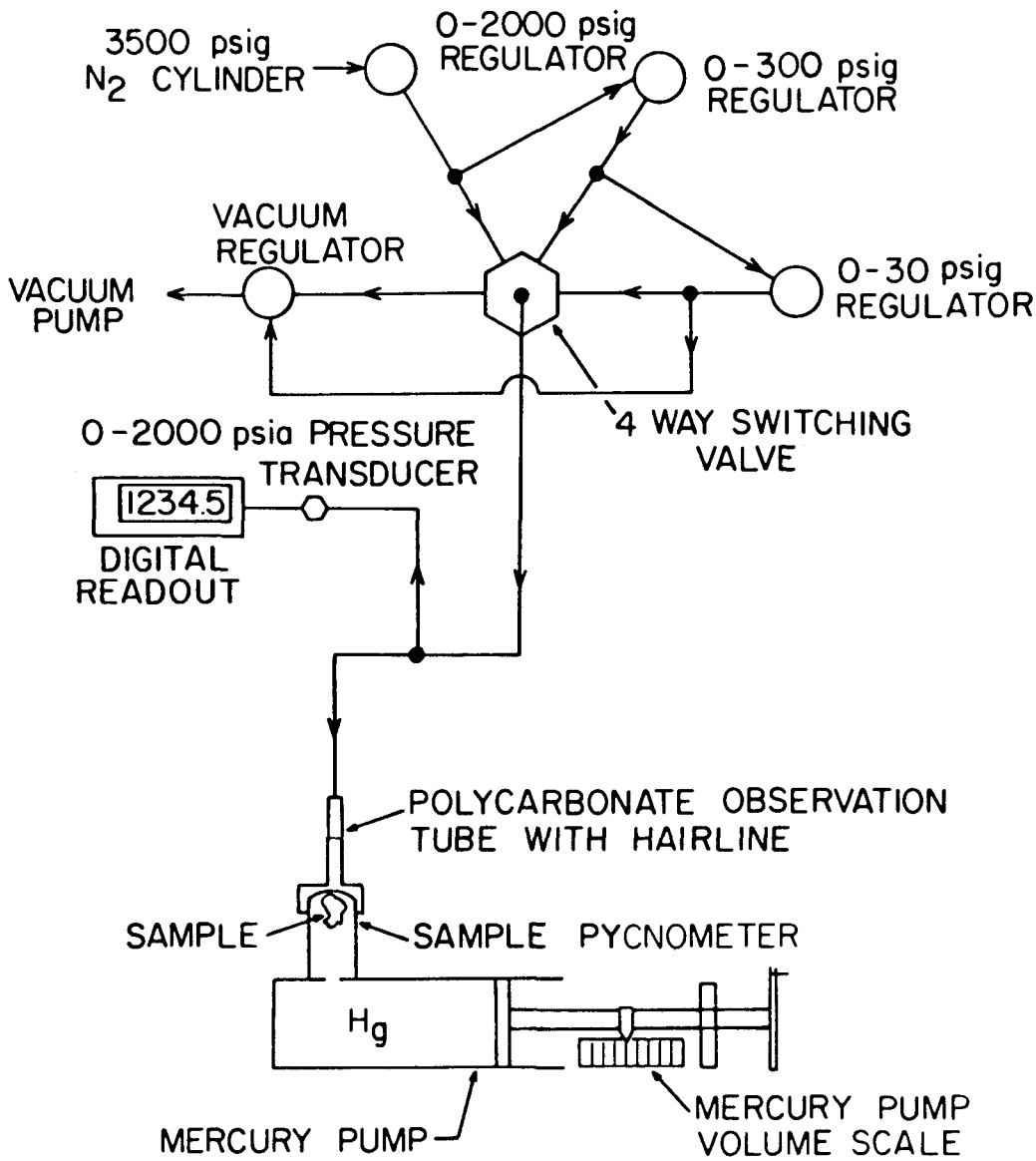

Fig. 20. Schematic drawing of the mercury infusion porosimeter.

Porosity and pore-size distribution measurements are made by placing a dried and weighed sample of tuff in the pycnometer and evacuating the system to <1 mm Hg. The mercury pump is used to force mercury into the pycnometer until the mercury level rises to a hairline in the observation tube. The displacement of the mercury pump piston is then read to 0.001 cm^3. The total displacement from the zero position gives the bulk sample volume because at 1-mm Hg pressure virtually none of the mercury will infuse into the sample.

In the past, the total sample porosity has been calculated from the sample weight and bulk volume using the average grain density of 2.301 ± 0.04 g/cm^3 reported by Manger[16] for tuffs from subunit T of the Paintbrush Tuff. We have ordered pycnometers for making grain density measurements ourselves and will use these values to obtain more accurate total porosity measurements in the future.

After the bulk volume has been determined, the pressure in the pycnometer is increased stepwise by releasing vacuum and applying N_2 gas pressure. After each step increase in pressure, the system is maintained at that pressure for several minutes to allow the mercury to infuse into the sample. The cumulative volume change is then measured by bringing the mercury level back to the hairline with the pump. Typically, 10 to 20 steps are used per order of magnitude change in pressure.

The pressure-volume (P-V) data are analyzed by subtracting the system volume expansion at each pressure from the cumulative volume change during the sample run and correcting for temperature changes. The system expansion correction is determined at low pressure using a semilog regression of the P-V data from the blank run. Above about 3.5×10^4 Pa, a linear regression equation is used for the system expansion correction. A P-V curve with the regression line for a typical blank run is shown in Fig. 21.

To date, pore-size distribution measurements have been made on samples HF23 and G1-2290. The computed total porosity of these samples was 40.2 and 28.8%, respectively. The theoretical pore diameters were calculated using the Washburn equation:

$$d_T = \frac{4\gamma\cos\theta}{P} \quad , \tag{7}$$

where d_T is the theoretical pore diameter, P is pressure, γ is the surface tension of mercury, and θ is the contact angle. The log pore-diameter vs cumulative percent porosity for these two samples is plotted on probability paper in Fig. 22.

Figure 22 indicates several significant differences between these two samples. First, whereas the median pore diameter (determined from the 50% porosity line) for sample G1-2290 is 3.9×10^{-5} cm, the median diameter for HF23 cannot be determined because it is $<10^{-5}$ cm. Extrapolating the

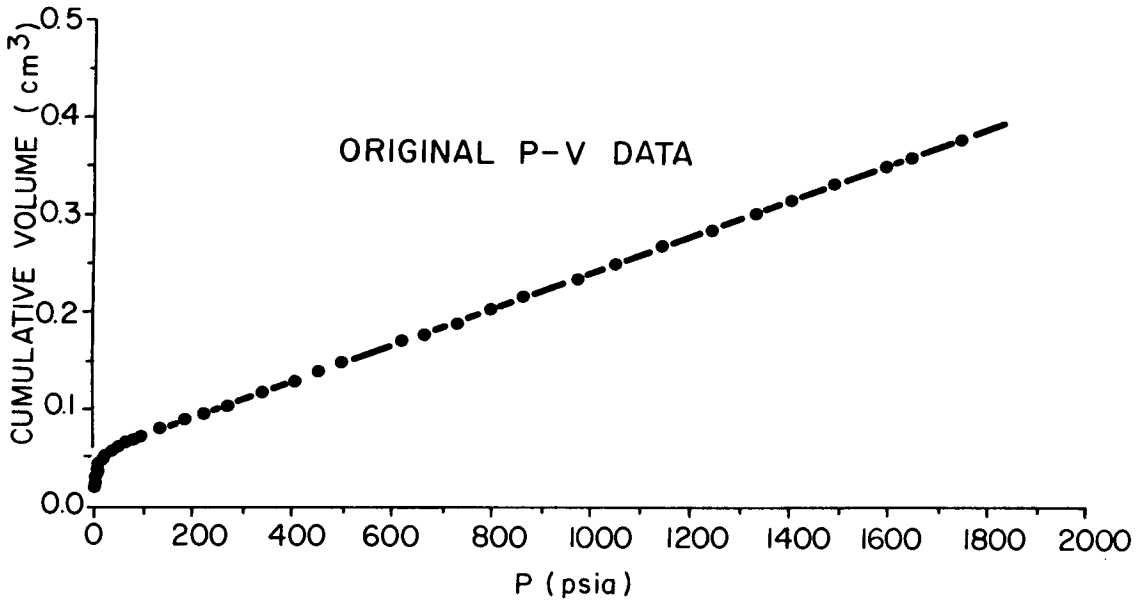

Fig. 21. Blank run P-V curve of the mercury infusion porosimeter.

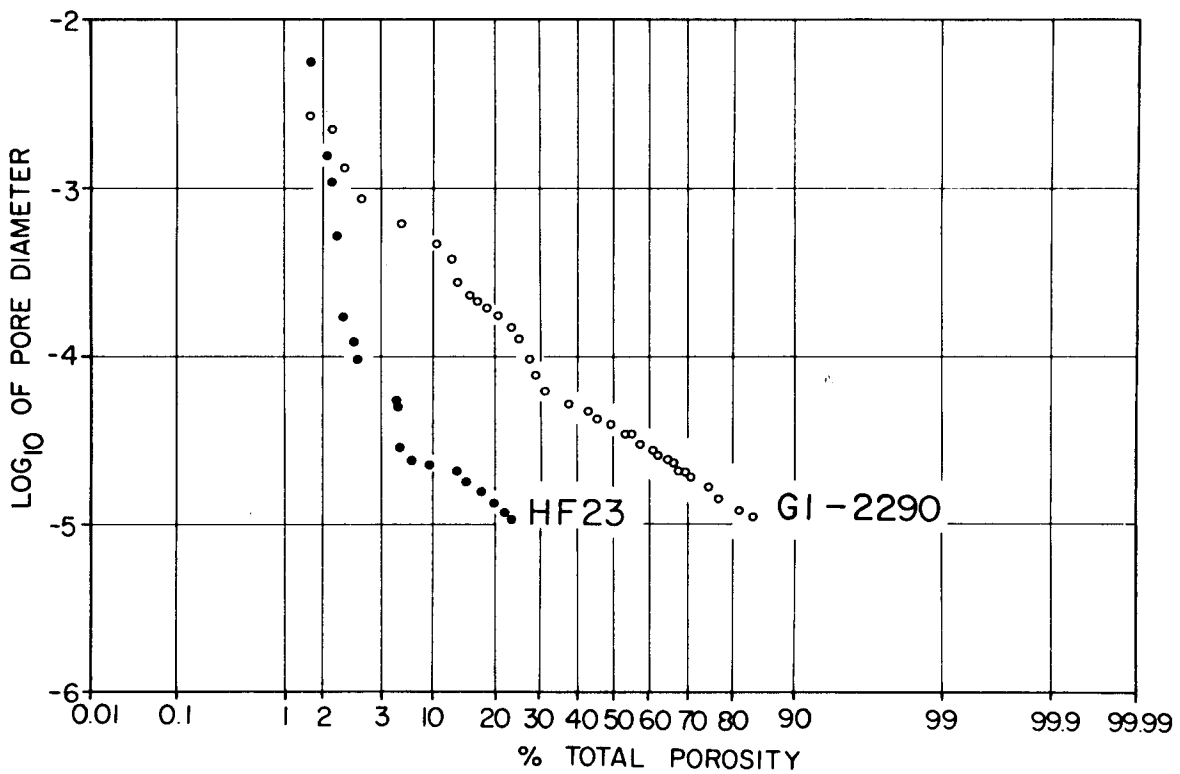

Fig. 22. Log of pore diameter vs percent of total porosity determined by mercury infusion porosity for samples HF23 and G1-2290.

line through the last six data points for sample HF23 suggests a median diameter of about 2.5 x 10^{-6} cm (0.02 μm). Assuming the total porosity calculations are valid, 85% of the total porosity of sample G1-2290 was >10^{-5} cm, but only 24% of the pores in sample HF23 are >10^{-5} cm. Lastly, the roughly linear trend of the data for sample G1-2290 on the probability graph indicates that pore-size distribution is approximately log-normal. The distribution for sample HF23 is very nonlinear although the smallest pores may approach a log-normal distribution.

b. Tuff Diffusion Studies. As reported previously,[1] diaphragm diffusion cells were designed and constructed to directly measure diffusion through discs cut from the tuffs. A drawing of the diaphragm diffusion cell is shown in Fig. 23. The diffusion experiments are performed by cementing a tuff disc, 1-in. diam by 0.25-in. thick, in the membrane-holding disc of the cell. A solution that has a high concentration of the diffusing species is placed in the lower reservoir, and a solution of lower concentration is placed in the upper reservoir. The resulting concentration gradient causes molecular diffusion through the tuff disc. All the solutions used in the tuff diffusion experiments are prepared using water from well J-13 as the solvent.

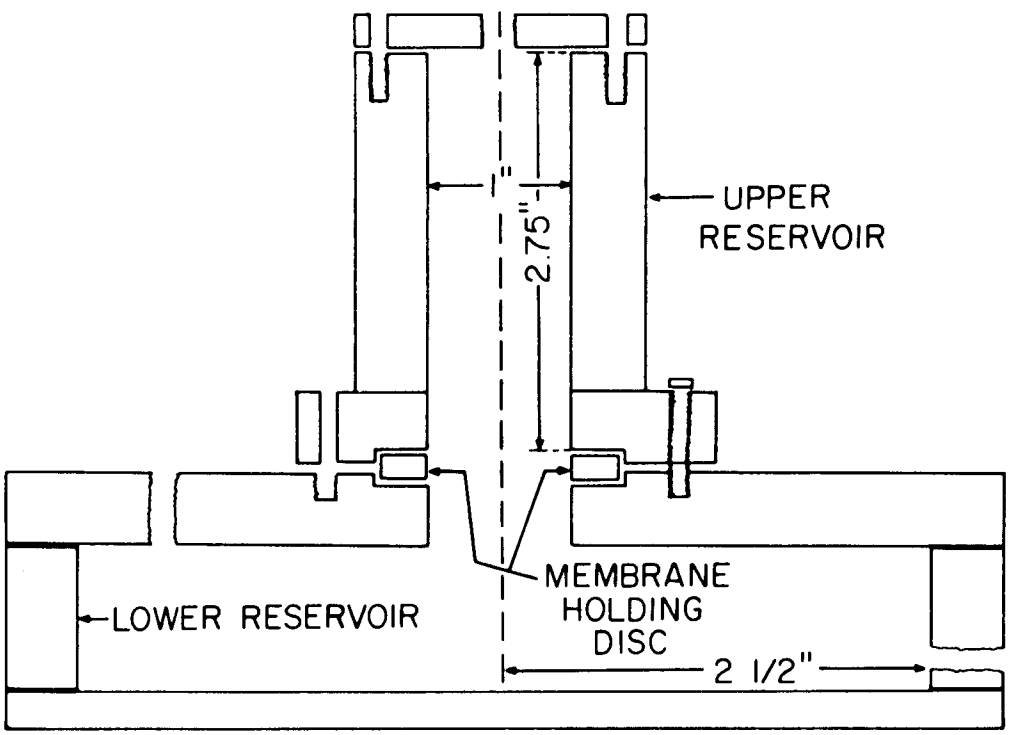

Fig. 23. Plexiglas diaphragm diffusion cell.

The concentration of the diffusing species is continuously monitored in the upper reservoir using the pumping and detection system shown in Fig. 24. The detector for the tuff diffusion studies consists of a Plexiglas flow-through cell into which a bromide ion-selective electrode and a reference electrode are inserted. The solution from the upper reservoir is pumped through the cell using a peristaltic pump. We had originally used a liquid chromatograph pump for this purpose, but found the peristaltic pump to be simpler to use and more reliable. Output from the ion-selective electrode is measured with a pH-millivolt meter, and an analog signal is recorded on a chart recorder.

To date, two diffusion experiments have been performed on sample U12G-RNM9 and one on sample G1-2290. The experiments were performed using solutions of

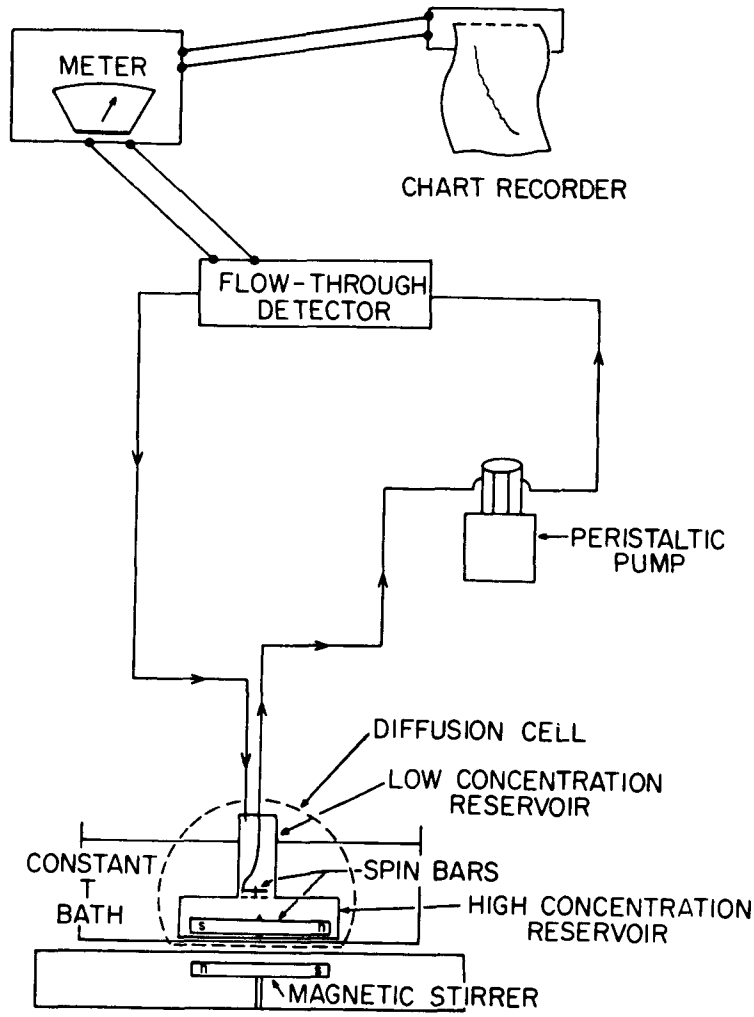

Fig. 24. Schematic drawing of the pumping and detection system of the diffusion cell.

NaBr in J-13 well water. Prior to the tests, the tuff discs were soaked in the NaBr solution for several days. To start the tests, the lower reservoir was filled with the NaBr solution and the tuff sealed in place in the diffusion cell. Vacuum was then applied to the upper reservoir to remove air from the disc and to initiate a flow of solution through the disc. Several hours were required to draw a few milliliters of solution through the disc. An additional quantity of NaBr solution was then poured into the upper reservoir, and the cell was placed in a constant temperature bath at (25.0 ± 0.1)°C for several hours prior to the test. This procedure was designed to assure that the pure fluid in the tuff disc was in equilibrium with the solution in the lower reservoir at the start of the test. The tests were initiated by removing all or part of the solution in the upper reservoir and replacing it with J-13 well water.

The resulting time-concentration data are analyzed using the so-called steady-state method.[17] This method uses only the data taken after a sufficient time has elapsed for an approximately linear concentration gradient to be established across the disc. When such a gradient has been established, the time-average diffusion coefficient is given by

$$\bar{D}_e = \frac{1}{\beta t} \ln \Delta C^* \quad , \tag{8}$$

where

$\bar{D}_e$ is the time-average effective diffusion coefficient,

β is a cell constant dependent on the surface area and thickness of the membrane and the volumes of the upper and lower reservoirs,

t is the time, and

ΔC^* is the ratio of the differences between the reservoir concentrations at time t_o when a linear concentration gradient has been established and at time t.

To compute ΔC^*, both the upper and lower reservoir concentrations must be known. The upper reservoir concentration is measured, and the lower reservoir concentration is computed from the change in upper reservoir concentration. In practice, the lower reservoir concentration changes by less than 1% during the course of the experiments.

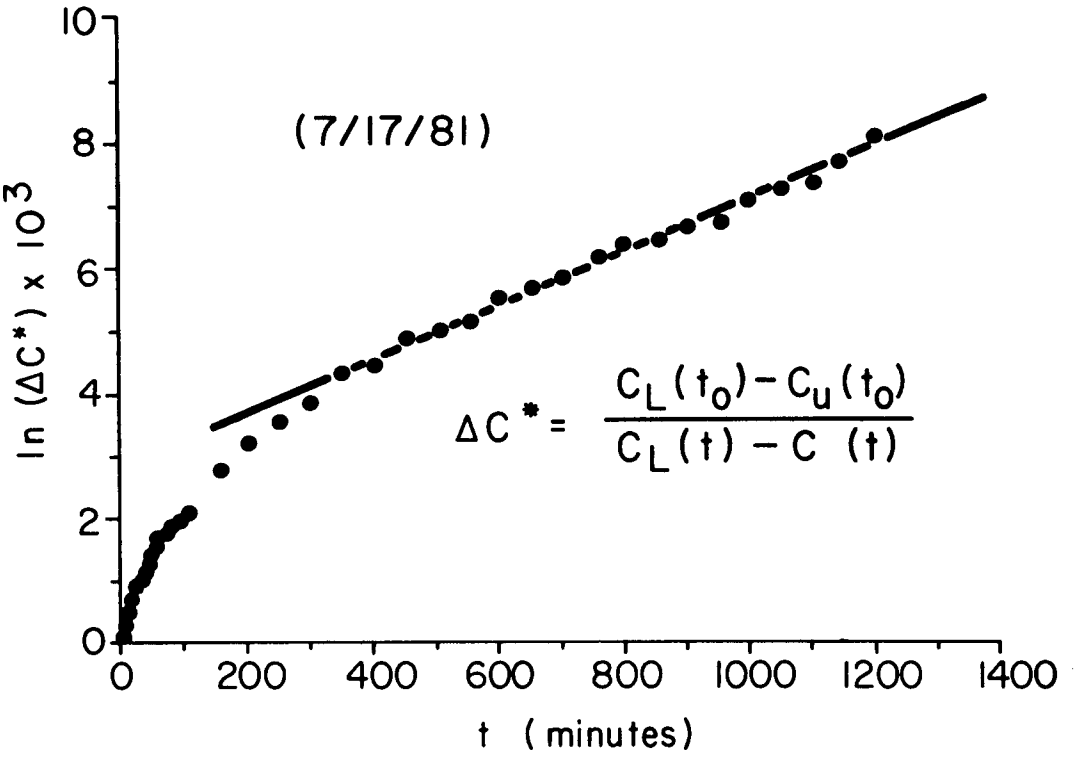

Fig. 25. Time-concentration curve from diffusion test on sample U12G-RNM9.

To apply the steady-state method, a time must be selected after which a linear concentration gradient is assumed. We determine this time by plotting $\ln\Delta C^*$ vs time as shown in Fig. 25 for sample U12G-RNM9. From this figure, we see that the $\ln\Delta C^*$ becomes linear in t after about 400 min. Regression analysis is then used to compute $\bar{D}_e$ from the linear portion of the curve.

Eventually, we will also analyze the nonlinear portion of the curve using the modified analytical solution of Spacek and Kubin.[18] Use of the nonlinear solution requires a special computer program, which we have yet to complete.

Using the techniques described above, the first diffusion test on sample U12G-RNM9 yielded an effective diffusion coefficient of $(7.6 \pm 0.2) \times 10^{-7}$ cm^2/s. The second test on the same disc performed 2 wk later yielded a value of $(3.70 \pm 0.03) \times 10^{-6}$ cm^2/s. The first test was performed with 0.02 M NaBr, and the second wth 0.05 M NaBr. The higher diffusion coefficient from the second test may be due to deterioration of the sealant around the tuff disc or deterioration of the tuff disc itself.

The diffusion test performed on sample G1-2290 yielded an effective diffusion coefficient of $(4.0 \pm 0.6) \times 10^{-7}$ cm^2/s. The NaBr concentration used in this experiment was 0.05 M. The ratio of the effective diffusion

coefficient to the free aqueous diffusion coefficient is about 3×10^{-2}. Porter and others[19] have related the effective diffusion coefficient to the free aqueous diffusion coefficient by the equation

$$D_{eff} = \alpha\theta(L/L_e)^2 D \quad , \tag{9}$$

where

D_{eff} is the effective diffusion coefficient,
α is an empirical correction factor,
θ is the porosity, and
L/L_e is the macroscopic diffusion length over the effective diffusion length (tortuosity).*

Using a porosity of 0.28 and a tortuosity of 0.70, we can compute α for the G1-2290 sample to be about 0.2. The factor α has been interpreted as a measure of ionic interactions with the electric double layer on the matrix grains and changes in pore fluid viscosity in small pores. If α is indeed a measure of ion-surface interactions, then it should be a function of the ionic strength of the test solutions. Double-layer theory predicts that α should decrease with decreasing ionic strength. At the ionic strength of well J-13 water (about 5×10^{-3} M), α and the effective diffusion coefficient might be considerably lower. We plan to test this prediction in the future.

3. Tracer Characterization. Experiments were begun to determine the acid dissociation constants of the fluorobenzoic acids, their complexing behavior, and their free aqueous diffusion coefficients.

a. Acid Dissociation Constants. Of the five fluorobenzoic acids we use as tracers (o-, m-, and p-fluorobenzoic acid, pentafluorobenzoic acid, and m-trifluoromethyl benzoic acid), we have found published values of pKa values for the first four.[20,21] These values are given in Table XXV. Two series of titrations were performed in an attempt to verify these values for our reagents. In both attempts, we could not reproduce the published values. Analysis of the problem was complicated by a malfunctioning pH meter. A titration system with a new pH meter has been designed so that the titrations can be performed

*L_e/L is the same as τ used in Sec. III.F. of this report.

TABLE XXV

PUBLISHED pKa VALUES FOR FLUOROBENZOIC ACIDS

Compound	pKa	Reference
o-fluorobenzoic acid	2.90	Kuhn and Wasserman[20]
m-fluorobenzoic acid	3.85	Kuhn and Wasserman
p-fluorobenzoic acid	4.04	Kuhn and Wasserman
pentafluorobenzoic acid	1.75	Ryan and Berner[21]

under a nitrogen atmosphere to minimize the effects of CO_2 contamination on the titration curves. We suspect, however, that part of the problem may be caused by residual acidic impurities in our reagents.

b. Complexing Behavior. To evaluate the possibility of complexing between the fluorobenzoate tracers and transition metals, a series of titrations was performed in which solutions of the sodium and potassium salts of the fluorobenzoates were added to solutions of Cu^{+2}, Ag^{+}, and Pb^{+2}. During the titrations, the metal-ion activities were monitored with their respective ion-selective electrodes. A complex series of reactions was observed that resulted in precipitation of either metal fluorobenzoate or metal hydroxides, depending on the pH of the solution. We also observed that the solubility of the metal fluorobenzoates increased with the acidity of the corresponding fluorobenzoic acid. We did not, however, observe changes in the metal-ion activities that might be interpreted as complexation or ion-pairing. For this reason, we have discontinued these studies.

c. Free Aqueous Diffusion Coefficients. Determination of the free aqueous diffusion coefficients of the fluorobenzoate tracers has been approached in two ways. First, the limiting ionic conductances of the anions have been measured and used to compute the diffusion coefficients at infinite dilution. Second, efforts are under way to directly measure the diffusion coefficients in concentrated solutions, using the diaphragm diffusion cells described earlier.

4. Limiting Ion Conductances. The limiting ionic conductance of an ion is defined as its equilvalent ionic conductance at infinite dilution. These values for the fluorobenzoate anions were determined by measuring the molar conductances of their sodium and potassium salts at various concentrations. For strong electrolytes such as these, the molar conductance is described by the empirical equation[22]

$$\Lambda = \Lambda_o^+ - k_c\, c^{1/2} \quad , \tag{10}$$

where

Λ is the molar conductance,
Λ_o^+ is the molar conductance at infinite dilution,
k_c is an experimental constant, and
c is the molar concentration.

The sodium and potassium salts of the fluorobenzoic acids were prepared by titrating the acids with the appropriate base to the equivalence points. The resulting salt solution was then used to prepare more dilute solutions. The conductivities of these solutions were then measured using the apparatus shown in Fig. 26. The temperature bath was set at (25 ± 0.05)°C. The values

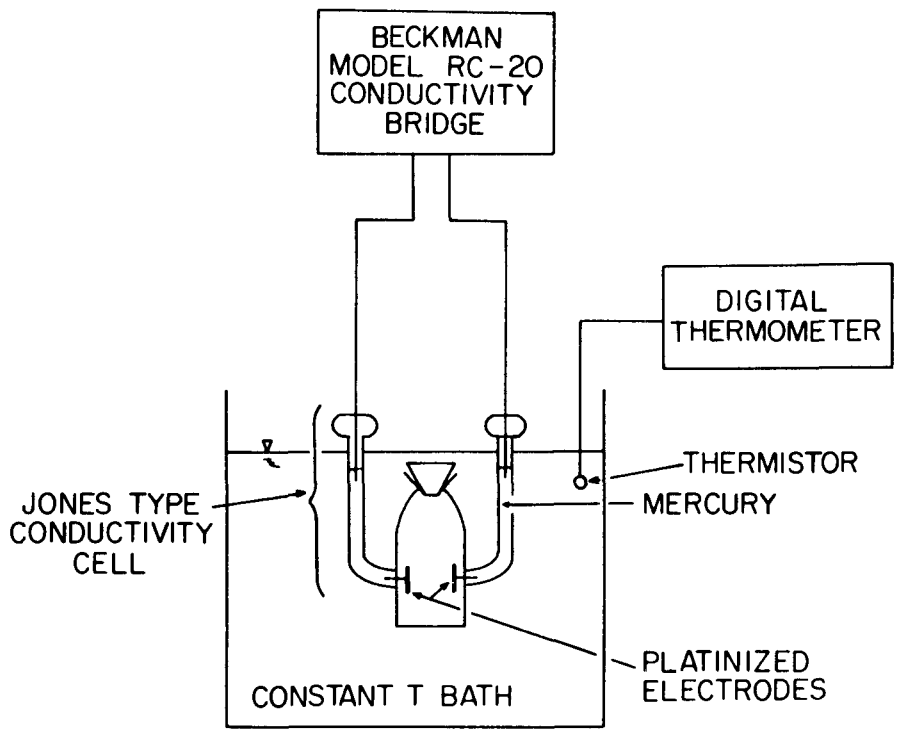

Fig. 26. Schematic drawing of apparatus used for electrical conductivity measurements.

of Λ_o for the salt solutions were determined by regression techniques. The limiting ionic conductance of the anion was then computed from the Kohlrausch's Law of the Independent Migration of Ions,[22]

$$\Lambda_o = \Lambda_o^+ + \Lambda_o^- \quad , \tag{11}$$

where Λ_o^+ values for sodium and potassium ions are known.

The resulting values for the limiting ionic conductances and computed diffusion coefficients are listed in Table XXVI. Based on the differences between the measured values and the published values for benzoate and p-fluorobenzoate, the error in the other measured values is estimated to be ~7%. We do not know the source of this error, but this level of accuracy seems adequate for our purposes.

5. Diffusion Experiments. Considerable effort was devoted during the second quarter to developing procedures for measuring diffusion coefficients of the tracers, using the diaphragm diffusion cell. Such experiments are

TABLE XXVI

LIMITING IONIC CONDUCTANCES OF BENZOATE AND FLUOROBENZOATES AND COMPUTED DIFFUSION COEFFICIENTS (D_o)

	$\Lambda_o \left(\frac{cm^2}{ohm\text{-}eq.} \right)$		
Species	Published	Measured	D_o
benzoate	32.38	30.8	0.82×10^{-5}
p-fluorobenzoate	33.00	35.0	0.93×10^{-5}
m-fluorobenzoate	-	30.0	0.80×10^{-5}
o-fluorobenzoate	-	30.5	0.81×10^{-5}
m-trifluoromethylbenzoate	-	27.9	0.74×10^{-5}
pentafluorobenzoate	-	27.1	0.72×10^{-5}

performed by sealing a sintered glass filter into the membrane-holding disc of the diffusion cell. The diffusion experiment is then conducted in the same way as the tuff diffusion experiments, except that the solvent is distilled water and a flow-through conductivity cell is used for a detector. In order to measure a diffusion coefficient in this way, diffusion experiments are first made with salts of known diffusion coefficients so that a cell constant can be computed. The cell constant corrects the apparent diffusion coefficient for the area, thickness, tortuosity, and porosity of the glass filter.

In our initial experiments, a medium glass filter was used, and we attempted to determine a cell constant using LiCl, NaBr, and KCl solutions. We were not able to obtain consistent cell constants using these salts, apparently because of convection through the filter caused by stirring the two reservoirs. We are now using a fine glass filter and have determined cell constants using LiCl and KCl that agree within 5%. We will soon begin diffusion experiments using sodium and potassium salts of the fluorobenzoates.

6. Numerical Modeling. The partial differential equations governing isothermal, multicomponent transport through a single fracture in porous rock have been formulated, based on the phenomenological equations of irreversible thermodynamics. The phenomenon of hydrodynamic dispersion in the fracture is included as a semianalytical term derived from the work of Taylor.[23] The governing equations are in such a form that they can be solved with integrated finite-difference methods. The equations were formulated to handle the phenomena of multicomponent diffusion into the matrix, osmotic and electro-osmotic effects, and ion filtration.

Multicomponent effects on transport caused by chemical reaction and complexation will be incorporated into the model, using an equilibrium distribution model based on the monotone sequences method of Wolery and Walters.[24] The equilibrium model has been developed and tested.

K. Diffusion into the Rock Matrix (R. S. Rundberg)

Kinetic sorption experiments (sorption as a function of time) have been performed on thin tablets of tuff (Sec. IV.D.). The uptake of activity has been measured as a function of time for a number of elements on several tuffs. These data should fit the solution for diffusion into a

plane sheet if one ignores any edge effect. The diffusion equation for this case is

$$\frac{\partial C}{\partial t} = D \frac{\partial^2 C}{\partial x^2} \quad , \tag{12}$$

with the initial conditions

$$C = 0, \; -\ell < x < 1, \text{ and } t = 0$$

and with the boundary conditions

$$a \frac{\partial C}{\partial t} = \pm D \frac{\partial C}{\partial x} \quad , \; x = \pm\ell \quad , \text{ and } t > 0 \quad ,$$

where

C is the concentration in solution,
D is the apparent diffusion coefficient,
a is the corrected depth of solution,
ℓ is half the thickness of the tablet (sheet),
t is the time, and
x is the position in the sheet.

In other words, the rate of loss of tracer from solution is equal to the rate at which tracer enters the sheet through the surfaces at $x = \pm\ell$.

The general solution to this problem is given by Crank.[25]

$$\frac{M_t}{M_\infty} = 1 - \sum_{n=1}^{\infty} \frac{2V(1 + V)}{1 + V + V^2 q_n^2} e^{-Dq_n^2 t/\ell^2} \quad , \tag{13}$$

where

M_t is the amount of solute in the solid phase at time t,
values of q_n are the nonzero positive roots of $\tan q_n = -V q_n$, and
$V = \frac{a}{K\ell}$, the solution-to-solid volume ratio divided by the partition factor K.

The fractional uptake of activity at equilibrium is given by

$$\frac{M_\infty}{2aC_o} = \frac{1}{1 + V} \quad . \tag{14}$$

If V is small, <0.01, which is the usual case for large K_d values, the following approximate relation may be used for early times.

$$\frac{M_t}{M_\infty} = 1 - e^{T/V^2} \text{ erfc } (T/V^2)^{\frac{1}{2}} \quad , \tag{15}$$

where $T = Dt/\ell^2$. A plot of this function is given in Fig. 27. This plot may be used to calculate the apparent diffusion coefficient, provided the K_d value is known. Thus, one should be able to estimate the constrictivity-tortuosity factor from these experiments.

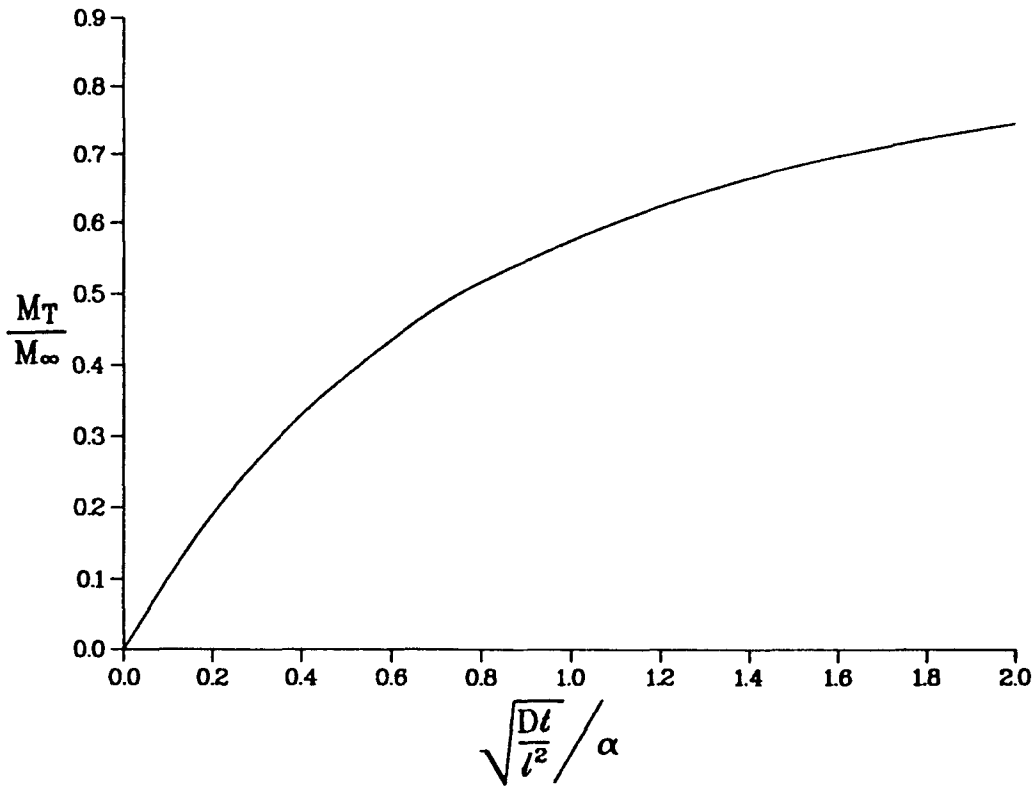

Fig. 27. Uptake of activity by a plane sheet for V < 0.01.

L. Modeling of Groundwater Interactions (J. F. Kerrisk)

Two, aqueous-chemical-equilibrium, computer programs are being made operational to aid in the investigation of groundwater interactions with stored wastes. A compiler for the PL/I language has been obtained for use with the NOS system of the Los Alamos CDC computers, and attempts were made to compile the WATEQ2 program.[26] However, the program uses a number of PL/I features that are not available on the CDC compiler. Two options, reprogramming WATEQ2 to be compatible with the CDC PL/I compiler and running on the Los Alamos WX Division IBM computer, are being investigated. The EQ3/6 computer program[27] is now running on the LTSS system of the Los Alamos computers. Test problems obtained with the program have been run.

Concentration data[15] taken in 1964 on a water sample from well J-13 have been used with four, chemical-equilibrium, computer programs, GEOCHEM,[28] REDEQL.EPAK,[29,30] WATEQF,[31] and EQ3/6. All programs indicated that the water was supersaturated with respect to some minerals; however, the predicted precipitates differed for GEOCHEM, REDEQL.EPAK, and EQ3/6. WATEQF does not predict precipitates; it merely indicates supersaturation. The variation in the results was caused by two differences among the programs. The programs do not consider the same group of solid phases; thus, a solid predicted to precipitate by one program may not even be considered by another. Also, the thermodynamic data for the solids and aqueous complexes differ among the various programs.

The mineral phases that will be encountered at Yucca Mountain are generally known. A review of available thermodynamic data of these minerals has been started.

V. MINERALOGY-PETROLOGY OF TUFF (D. L. Bish, F. A. Caporuscio, P. R. Carroll, B. M. Crowe, and K. Lombardo)

A. Clay Mineral Stability

An August 1 milestone was met by the submittal of a detailed report on the clay mineralogy of the Bullfrog and Tram Members in the USW-G1 drill core. This report[32] concludes that the swelling properties of sodium-saturated smectitic clays are important to characterize because of possible changes in geochemical or thermochemical rock and mineral properties. Basal spacings in

montmorillonite-beidellites range from 10 Å at 0% relative humidity to 20 Å at 100% relative humidity. Swelling pressures of clays within these humid conditions are about 4 x 10^9 dyne/cm^2. These pressures could be important in the sealing or opening of fractures under hydration-dehydration conditions. Minor heating of tuff with dehydration may result in the collapse of smectitic clays, opening fractures and releasing water. However, the highly expandable sodium-saturated smectite-beidellites that occur throughout the tuff could equally act as efficient barriers to fluid flow, immediately swelling in a hydrous atmosphere and effectively controlling permeability. The clays may have quite variable effects depending upon whether they occur in fractures, lining pores in the groundmass, or as massive alteration products of pumice fragments. These complexities of occurrence indicate that careful field experiments are as important as controlled laboratory experiments in the understanding of clay alteration.

Sodium-saturated smectites commonly exhibit basal spacings of approximately 19.5, 15.6, 12.6, and 10 Å with decreasing humidity, demonstrating the existence of, respectively, three, two, one, and no layers of water between the tetrahedral-octahedral-tetrahedral smectite sheets. Under room conditions (20 to 50% relative humidity, 20 to 25°C), all of the smectites examined from the Bullfrog and Tram units have one layer of interlayer water yielding basal spacing of approximately 12.6 Å. These conditions certainly do not represent those occurring in the rocks as both the Bullfrog and Tram Members are in the saturated zone with temperatures ranging from approximately 35°C to 45°C (Ref. 33). Solvating the montmorillonites with water and allowing them to dry before x-raying reveals that all of the montmorillonites examined expand to approximately 20 Å in a 100%-relative-humidity atmosphere and, as they dry, contract to approximately 12.6 Å, going through a 15-Å intermediate state. The behavior of these montmorillonites is typical of sodium-saturated smectites. There are, however, minor fluctuations in the spacings of the different hydrates, probably as a result of variations in layer charge and in the interlayer cation. Depending on the exact conditions present in the rocks, the montmorillonites can have quite a large variation in basal spacing and, consequently, in molar volume.

Further information on the behavior of the montmorillonite-beidellites when heated can be obtained by heating samples to 200°C and resolvating with ethylene glycol. Samples with relatively highly charged layers and appreciable

interlayer potassium will expand only partially, or not at all, after this treatment. Sample G1-3196, from the 974.1-m depth in the USW-G1 core, was the only sample to be affected by heating, only partially expanding in ethylene glycol. Heating this sample to 100°C had no effect on the expansion behavior. In addition, potassium saturating and heating the montmorillonite-beidellite in G1-3500 had no effect on the expansion properties. The montmorillonite-beidellites in the Bullfrog and Tram Members have typical layer charges (about 0.33) and few or no high-charge layers. This suggests that the cation exchange capacities will not be substantially altered by heating up to 200°C.

As noted above, during diagenesis, smectites commonly undergo an irreversible transition to illite through an interstratified illite-smectite intermediate. The extent of this reaction in pelitic sediments can be used as an approximate geothermometer,[34,35] and it is thus essential to examine the extent of this reaction in the tuffs at the Nevada Test Site (NTS). The degree of interstratification in the montmorillonite-beidellites was examined. Using the techniques of Reynolds et al.[36] and Srodon,[35] Table XXVII lists the results of these determinations along with the approximate ethylene glycol complex layer thickness. In all samples, the montmorillonite-beidellites are randomly interstratified with a small proportion of illite, and no ordered interstratifications are present. In all samples with low clay mineral contents, the degree of interstratification was estimated using the relative intensity of the low-angle scattering. However, this technique is beset by numerous problems connected with crystallite size and instrumental factors,[36] and these results are only qualitative. Srodon's methods[35] were applied to samples with more than 5% smectite, and these results are considerably more accurate; the uncertainties applied in Table XXVII for these smectites are conservative. It is obvious from these results that there is no consistent trend in the degree of interstratification with depth, and the amount of illite is fairly uniform throughout the Bullfrog and Tram Members, averaging about 10 ± 10%. There is some variation in the thickness of the ethylene glycol complex reflecting changes in the layer charges of the montmorillonite-beidellites.

In the tuffs, the diagenetic transformation from smectite to illite has proceeded only slightly, if at all, and this is contrary to expectations based on the maximum paleogeotherm[33] and observations in pelitic sediments. Reported[33] zeolite zone boundaries suggested temperatures between 75°C at the top of the Bullfrog Member and 110°C at the bottom of the Tram Member. The temperature

TABLE XXVII

X-RAY DIFFRACTION RESULTS FOR RANDOMLY INTERSTRATIFIED ILLITE-SMECTITES IN USW-G1

Sample Number	Depth (m)	Percent Illite in Illite-Smectite	Ethylene Glycol Complex Thickness (Å)
G1-2198	670.0	20 ± 10	16.90
G1-2318	706.5	20 ± 10	16.80
G1-2349	716.0	25 ± 10	16.70
G1-2436	742.5	20 ± 10	16.75
G1-2467	751.9	20 ± 20[a]	n.d.[b]
G1-2486	757.7	20 ± 20[a]	n.d.
G1-2525	769.6	25 ± 20[a]	16.70
G1-2613	796.4	30 ± 20[a]	16.75
G1-2622	799.2	30 ± 20[a]	n.d.
G1-2641	805.0	30 ± 10	16.80
G1-2715	827.5	30 ± 20[a]	n.d.
G1-2748	837.6	10 ± 10	16.80
G1-2804	854.7	30 ± 20[a]	n.d.
G1-2820	859.5	10 ± 10	16.70
G1-2868	874.2	30 ± 20[a]	n.d.
G1-2884	879.0	30 ± 20[a]	n.d.
G1-2932	893.9	30 ± 20[a]	n.d.
G1-2981	908.6	30 ± 20[a]	n.d.
G1-3001	914.7	10 ± 10	16.70
G1-3039	926.3	30 ± 20[a]	n.d.
G1-3099	944.6	5 ± 5	16.75
G1-3137	956.2	15 ± 10	16.75
G1-3196	974.1	20 ± 10	16.75
G1-3238	986.9	10 ± 10	16.85
G1-3258	993.0	25 ± 10	16.90

TABLE XXVII (Cont.)

X-RAY DIFFRACTION RESULTS FOR RANDOMLY INTERSTRATIFIED ILLITE-SMECTITES IN USW-G1

Sample Number	Depth (m)	Percent Illite in Illite-Smectite	Ethylene Glycol Complex Thickness (A)
G1-3321	1012.2	10 ± 10	16.90
G1-3345	1019.6	5 ± 5	16.90
G1-3371	1027.5	15 ± 10	16.90
G1-3468	1057.0	5 ± 5	16.85
G1-3500	1066.8	5 ± 5	16.90

[a]Estimated from low-angle scattering.

[b]n.d. not determined.

currently ranges from 35 to 45°C. It thus appears that either 1) the reaction kinetics in the tuffs are significantly slower than in typical pelitic sediments, or 2) the smectites in the tuffs result from later alteration at temperatures more closely approaching the current geotherm than the maximum paleogeotherm. The reaction of smectite to interstratified illite-smectite has been shown[37] to be significantly inhibited by sodium, calcium, and magnesium in solution in addition to potassium. Indeed, Wolfsberg et al.[7] reported considerably more calcium (13 meq/ℓ) and sodium (50 meq/ℓ) than potassium (4.7 meq/ℓ) in the water from well J-13. It is therefore probable that the solution chemistry in the tuffs has a pronounced effect on the rate of the smectite to illite-smectite reaction. Considering the relatively steep paleogeotherm, it is equally likely that the smectites formed under conditions more closely approaching the present; smectites are typically only 20% expandable[38] by 100°C in Gulf Coast sediments. It appears certain that the zeolites and smectites formed under separate conditions and at different times in the tuffs at the Nevada Test Site.

Petrographic studies of smectite occurrence indicate that swelling clays are common throughout the drill core, with local abundances as high as 30%. Smectites are present in all samples of the Tram examined here; the upper part (805.0-914.4 m) contains small amounts of smectites, but below 914.4 m, the

Tram is fairly rich (up to 30%) in smectites. There are no consistent correlations in the Bullfrog and Tram Members between the amounts of smectites and the amounts of zeolites, quartz, and alkali feldspar. In some intervals, the zeolitized zones are the poorest in smectite (Bullfrog), while in others (lower Tram), relatively abundant smectites and zeolites occur together. Smectites are present equally in welded and nonwelded horizons and, contrary to expectation, are scarce in some zones with absent or slight welding and probably high original permeability (Bullfrog Member, 762.0 to 792.5 m). The absence of smectites in non-welded, zeolite-rich horizons may be due to lowering of the permeability by zeolites. If so, this indicates that the formation of the smectites postdates zeolite growth in the tuffs.

Many questions remain regarding the importance of clay stability in repository construction and siting. What is the extent of hydration-dehydration alteration in natural smectites using waters that occur at Yucca Mountain? Are layer charges and swelling capacity altered at elevated temperature when smectites are exposed to the naturally occurring or waste-cation-doped waters? What alterations in rock strength can be expected? What alterations in porosity and in permeability can be expected from clay alteration? The qualities of strength, porosity, and permeability can be approached by laboratory studies but ideally require field experiments for proper scaling.

B. X-ray Diffraction Studies of Soak Test Samples

Preliminary x-ray diffraction studies of the soak test samples were made during this quarter. In general, there were few noticeable changes even in samples that were run for 3.5 months at 180°C. Because the apparent lack of alteration included zeolite-free samples of the Topopah Springs unit, subjected to conditions well within the range of zeolite stability, the negative results are an indication that zeolite-forming reactions are very sluggish in these samples. A similar conclusion might be extended to the apparent absence of analcime in any of these experimental runs. Alternatively, these minerals may have formed in small amounts below the resolution of detection by x-ray diffraction. Detailed petrographic and SEM studies will pursue this latter possibility.

The results of x-ray diffraction studies of the soak test samples are summarized in Table XXVIII. Samples of the Topopah Springs unit show no detectable change. There may be slight decreases in the zeolite, alkali feldspar, or

TABLE XXVIII

RESULTS OF X-RAY DIFFRACTION STUDIES OF SOAK TEST SAMPLES

Sample (depth in ft)	Mineralogy	Temp. (°C)	Observed Change[a] 2[b]	2.5	3.5	5	6
Topopah Springs							
(1090)	alkali feldspar, mica, quartz, cristobalite	120		n.c.		n.c.	
(1101)	alkali feldspar, mica, quartz, cristobalite	180			n.c.		
(1106)	alkali feldspar, mica, quartz, cristobalite	80					n.c.
Calico Hills							
(1668)	mordenite, cristobalite, quartz,	120		mordenite			
Bullfrog[c]							
(2381)	alkali feldspar, quartz, smectite, mica	180			feldspar mica		
Tram							
(2773)	alkali feldspar, quartz, mica, cristobalite, clinoptilolite	120	feldspar SMECTITE				

[a]Symbol n.c. stands for no observable change in x-ray diffraction pattern. Lower-case mineral names indicate relative decrease of that mineral abundance; upper-case mineral name indicates relative increase in that mineral abundance.

[b]Duration of experiment in months.

[c]This sample alone was run in well J-13 water; all others in pure water.

mica contents of Calico Hills and Bullfrog samples, although the differences observed could be due to sample variability. The only strong changes observed occurred at 2 months and 120°C in the Tram unit, where there was a notable decrease in alkali feldspar and an increase of ~10 to 20% in smectite content. These changes in the Tram composition are greater than can be explained by sample heterogeneity.

The results of these x-ray diffraction studies indicate the importance of slow reaction kinetics and disequilibrium in mineral reactions such as might be expected in the far field, and perhaps even in the near field, repository environments. Many reactions of possible importance can be pursued in the laboratory, but the results of such experiments are likely to involve disequilibrium reaction products. For this reason, it would be advisable to design field experiments to run parallel with laboratory work. Field experiments would not have a serious impact on NNWSI program goals; in effect, the Test Evaluation Facility may be considered as a field experiment if properly located, operated, and examined.

VI. VOLCANISM STUDIES (B. M. Crowe, D. T. Vaniman, F. V. Perry, and W. S. Baldridge)

A. Redetermination of Areal Distribution in Probability Calculations

Final area-size determinations have been completed for volcanic probability calculations using the data base from the regional geologic mapping studies of basaltic volcanism in the southcentral Great Basin. A statistical procedure has been developed to determine the area ratio for the probability calculations. This procedure generates a minimum ellipse and minimum circle that enclose specified Quaternary basaltic centers. In this manner, the area ratio for the probability calculations is determined by the distribution of Quaternary volcanic centers, rather than by a circle of an arbitrarily determined radius with a center at the Yucca Mountain exploration site. The variation in area of these minimum ellipses and circles can be examined for different basaltic centers. The smallest areas correspond to the case of considering only the Quaternary basalt cones of Crater Flat, Lathrop Wells, and Sleeping Butte ($C_a = 2.4 \times 10^3$ km^2 and $E_a = 1.5 \times 10^2$ km^2 where C_a is the circle area and E_a is the ellipse area). The ellipse area is invalid and will be recalculated, as it does not include the Yucca Mountain site. A second, and probably more valid

area distribution, includes the basalt of Buckboard Mesa (C_a = 2.5 x 10^3 km^2 and E_a = 1.9 x 10^3 km^2). Both the ellipse and circle enclose the Yucca Mountain site, and factoring these areas into the probability calculations of Crowe and Carr[39] increases the final value by less than 60%. The circle and ellipse areas based on all Quaternary basalt centers in the northeast-trending volcanic belt are, respectively, 8.5 x 10^4 km^2 and 1.6 x 10^4 km^2. Finally, the circle and ellipse areas for all Quaternary basalt cones of the southcentral Great Basin are 8.5 x 10^4 km^2 and 6.6 x 10^4 km^2. The expanded ellipse for all Quaternary cones reflects strong deviation from a linear structure once volcanic centers outside of the northeast-trending volcanic belt are included.

B. Completion of Field Studies, Crater Flat Area

During July, field mapping and sample collection were completed in the Lunar Crater area and in contiguous parts of the Pancake Range in Central Nevada. The Lunar Crater basalt field is the northernmost member of the northeast-trending belt of basalt fields that includes Crater Flat. Previous field studies of the Lunar Crater area concentrated on the relatively young cones and flows of the central field. These younger basalts include highly nepheline-normative samples that may include abundant xenoliths and xenocrysts. The field studies in July continued to the south, covering the complete Lunar Crater volcanic field and including the Southern Pancake Range. Many of the flows sampled have high abundances of modal olivine (5 to 8% olivine phenocrysts). Similar olivine-rich flows occur among the younger basalts in the central field; basalt flows of the same type also cap Black Mesa, northwest of the central Lunar Crater area (dated at ~10 Myr). The field evidence suggests that these olivine-rich basalts, with few or no xenoliths and xenocrysts, have been erupted episodically over the last 10 Myr. Further petrographic and chemical studies will determine the chemical variability over time within this basalt type.

Included among the basalt lavas near Citadel Mountain are feldspathic units with abundant plagioclase phenocrysts. Isolated flows high in the southern Pancake Range are studded with abundant black clinopyroxene megacrysts. These feldspathic and black-clinopyroxene-rich basalts are similar to basalt units in the Reveille Range, and suggest petrogenetic continuity between basalt magma types in the Pancake and Reveille Ranges during late-Cenozoic time.

C. Petrologic Studies

Samples of basaltic ash were collected from a fault within alluvium at Crater Flat by W. Carr of the USGS. Correlation of the ash with a specific volcanic cycle may provide control on the age of fault movement. The ash differs from other samples of the basalts of Crater Flat in that the ash samples are very glassy (>50% glass) and lack clinopyroxene. The absence of clinopyroxene and the vitrophyric texture suggest rapid undercooling, to the extent that pyroxene did not nucleate.

The ash samples are olivine-porphyritic (Fo_{77}), with abundant acicular groundmass plagioclase ($An_{67}Or_1$ to $An_{52}Or_4$). Petrographically these samples cannot be related to the oldest basaltic volcanic cycle at Crater Flat (3.7 Myr), in which clinopyroxene and plagioclase phenocrysts are abundant. The two younger volcanic cycles (1.1 and 0.3 Myr) are both possible sources for the ash. Although the 0.3-Myr age cannot be ruled out, the distance to the 0.3 Myr center and the more calcium-rich feldspars of that center make it an unlikely source for the ash. A tentative 1.1-Myr age for the ash is suggested.

Petrographic studies during the quarter included an overview of the xenolith-bearing basalts within the NTS region. Basaltic hosts for xenoliths include the 7- to 9-Myr-old localities of Silent Canyon, Nye Canyon, and the northern Dome Mountain area. The most common xenolith types for all localities are gabbroic, containing plagioclase and clinopyroxene, often with olivine (relict) and rarely with orthopyroxene. Clinopyroxenites and troctolites also occur. Xenolith studies will be integrated into the petrologic history of basaltic volcanism in the NTS region.

D. Strombolian Eruptive Models

Basaltic eruption resulting in Strombolian scoria cones has been modeled by Crowe et al.[40] Eruptions are considered to have depths of magma origins of ~35 km, surface magma viscosities of 10^2 to 10^3 P, volatile exsolution depths of <2 km, and magma rise rates of 0.1 to 1.0 m/s. Typical volumes of Strombolian eruptions are 10^{-1} to 10^{-3} km^3. Volatile diffusion rates are high, allowing development of zones of high bubble concentration and coalescence near the surface immediately preceding eruption. A common sequence of explosive phases is recognized in the deposits and places constraints upon the mechanisms of Strombolian activity. All phases, here identified by major features, may

not occur in one eruption but usually do occur in the same sequence: 1) opening phase—short eruptive fissure, focusing down to one or two sites of effusion; 2) cone building phase—maximum scoria fall dispersal; 3) lava flow phase—most voluminous, highest magma flux rates; 4) cone modification phase; 5) dyke injection and late flow phase; 6) late mildly explosive phase—agglutinate rims. Phases 3 to 5 may be repeated through several cycles of activity. Strombolian eruptions of this nature have been characteristic of the past basaltic volcanic history of the NTS region (following the cycles of silicic volcanism). Any future basaltic eruptions might also be expected to be Strombolian in nature.

VII. ROCK PHYSICS STUDIES (J. D. Blacic, J. Carter, P. M. Halleck, P. Johnson, T. J. Shankland, R. Anderson, and K. C. Spicochi)

The results of half a year's soak tests first became available this quarter. The mineralogical studies are still very preliminary; initial interpretations are discussed above in Sec. V. Alterations in physical strength are discussed here.

The soak tests were designed to test a large number of samples for extended exposure to the hot, wet, high-stress conditions expected near a waste repository. The individual tests were designed to cover a range of temperature and pressure conditions simulating varying distances from the waste canister and different repository depths. Because the properties of tuffs vary substantially with lithology, a range of lithologic "types" covering varying degrees of welding and postdeposition mineralization was studied.

Samples for this study were selected from core taken from one of two test holes at the Yucca Mountain site at the Nevada Test Site. These holes are UE25a-1 and USW-G1. Four units were selected for these tests: Topopah Springs (UE25a-1), Calico Hills (UE25a-1), Bullfrog (USW-G1), and Tram (USW-G1). These selections were made to provide contrasting degrees of welding and zeolite content.

The samples exposed to high-temperature, high-pressure conditions were 2.54-cm-diam by 6.5-cm-long cylinders. Control samples came from the same piece of core as the test sample, in most cases cut side by side. Test conditions were chosen to simulate different burial depths, water table levels, and distances from the waste canisters. The three temperatures used (80, 120, and 180°C) reflect current targets for average formation temperatures and cover

the effect of possible underestimates. Confining pressures of 9.7 and 19.7 MPa simulate burial at 1500 and 3000 ft., respectively, and the differential pore-water pressures of 0.5 and 9.7 MPa correspond to above- and below-water table conditions. However, most tests were run with pore pressure equal to confining pressure.

Exposure times for the soak tests ranged from 2 to 6 months. Changes in tensile strength, compressive strength, porosity, and grain density vary with the temperatures of confinement and, more significantly, with the tuff type under study. The results for 80°C, 120°C, and 180°C experiments are summarized below. All results were treated by t-test statistics, and are thus rated as significant or nonsignificant.

A. Results at 80°C

1. Topopah Springs. There was no significant change in the tensile strength of rock from the 681-ft depth exposed at 9.7-MPa confining pressure for 6 months. However, for rock from 1106 ft exposed at 19.7-MPa confining pressure, there was a significant increase of 37% in tensile strength.

A decrease in compressive strength of 25% for rock from 1248 ft exposed at 9.7-MPa confining pressure was marginally significant. An apparent decrease of compressive strength of rock from 1100 ft exposed at 19.7-MPa confining pressure was statistically insignificant.

There was little or no change in grain density but a consistent increase in porosity.

2. Calico Hills. There were essentially no changes in tensile or compressive strength of Calico Hills tuffs at these exposure conditions. Both porosity and grain density appear to have increased slightly.

B. Results at 120°C

1. Topopah Springs. There was a significant decrease of 15% in the tensile strength of rock from the 730-ft depth exposed at 9.7-MPa confining pressure. An apparent increase in tensile strength at these conditions for rock from the 680-ft depth was not significant. At 19.7-MPa confining pressure, rock from the 708-ft depth showed a significant decrease of 34% in tensile strength, and there was a marginally significant decrease of 26% for rock from the 1090-ft depth.

None of the slight changes in compressive strength at 9.7-MPa confining pressure was significant. At 19.7-MPa confining pressure, there was a significant increase in compressive strength of 69% for rock from the 1090-ft depth

This contradicted a marginally significant decrease of 14% for rock from 1101 ft. Inconsistencies such as this are to be expected for a small number of tests in a rock that is highly inhomogeneous.

This inconsistency was even more apparent in porosity measurements, especially for samples exposed at 19.7 MPa. For the rock from the 708-ft depth, porosity decreased 12%, while for rock from 1090 ft it increased 8%. Grain densities either remained the same or increased slightly.

2. Calico Hills. There was a marginally significant increase of 16% in tensile strength for exposures at 9.7-MPa confining pressure; the changes for exposures at 19.7 MPa were insignificant.

Compressive strength consistently decreased up to 25% for exposures at both 9.7- and 19.7-MPa confining pressure, but these changes were only marginally significant.

The most consistent changes occurred in grain density and porosity, both of which increased from 5 to 19% at both confining pressures.

3. Bullfrog. The Bullfrog tuffs exhibited the lowest tensile strengths of all the units tested. There was a further marginally significant decrease of 8% for exposures at 9.7-MPa confining pressure. A slight decrease for exposures at 19.7-MPa confining pressure was statistically insignificant.

Compressive strength decreased 17% for exposures at 9.7-MPa confining pressure and 5% at 19.7 MPa. Both changes were judged to be statistically significant.

Grain densities were unchanged. Porosities were unchanged or slightly increased.

4. Tram. Results for Tram tuffs were almost identical to those of Bullfrog. Tensile strength decreased 30% for exposures at 9.7-MPa confining pressure. This change was judged to be statistically significant. The slight change at 19.7-MPa confining pressure was insignificant.

Compressive strength decreased up to 25% in a manner similar to that for Bullfrog tuffs; however, the tests were not statistically significant in this case.

Grain densities remained unchanged. Porosities decreased up to 9% for exposures at both 9.7- and 19.7-MPa confining pressures.

C. Results at 180°C

1. Topopah Springs. Tensile strength was 46% lower after exposure at 9.7-MPa confining pressure for 3.5 months. This reduction was statistically significant.

Compressive strength was reduced 8% in a single test at 9.7-MPa confining pressure.

Porosity decreased 38% and grain density increased slightly.

2. Topopah Springs Vitrophyre. Tensile strength was 23% lower after exposure of the glassy vitrophyre sample at 9.7-MPa confining pressure. The change was judged to be statistically significant.

Compressive strength changed slightly with no statistical significance.

The small initial (crack?) porosity decreased 22% with no change in grain density.

3. Calico Hills. Tensile strength apparently increased slightly, but this was not statistically significant. Similarly, compressive strength appeared to be lower after exposure, but this change was also judged not to be statistically significant.

Porosity was unchanged and grain density increased slightly.

4. Bullfrog. Tensile strength was up to 15% higher after exposure at 9.7-MPa confining pressure. Although this increase is small, it was judged to be statistically significant.

Compressive strength was up to 31% higher after exposure at 9.7-MPa confining pressure. Although this increase is small, it was judged to be statistically significant.

Grain density remained unchanged, but porosity decreased slightly.

5. Tram. Tensile strength was up to 36% higher after exposure at 9.7-MPa confining pressure. This change was judged to be statistically significant.

Compressive strength appeared to increase slightly; however, these changes were not statistically significant.

Grain density remained unchanged, but porosity was up to 8% higher after exposure.

VIII. EXPLORATORY SHAFT (D. C. Nelson, T. J. Merson, P. L. McGuire, J. W. Neudecker, and W. L. Sibbitt)

The preparation of the Exploratory Shaft (ES) conceptual design is continuing with a draft report scheduled to be completed by October 30, 1981.

The conceptual design is based on an assumed location and depth of the shaft and size of the underground test chamber. As more surface exploration data are collected, these assumptions may change and could have a significant effect on the current ES project costs and schedule. Special conceptual design studies have been completed by the NTS supporting contractors on shaft casing and drilling operations, shaft internals, exploratory openings, siteplan, ventilation system, and utility requirements. Additional information has been requested updating some of the cost estimates and schedules and comparing large-diameter shaft drilling operations with mining operations.

Santa Fe Engineering and Construction Company has developed technology for large-shaft drilling and casing techniques and would like to demonstrate the acceptability of this technology. They have proposed that they drill and case the ES on a cost-sharing basis as a means of demonstrating their technology. Two meetings were held with Santa Fe representatives to discuss their proposal. Comparison cost and schedule studies are now being performed; however, at a first look, it appears there would be little, if any, economic advantage to the NNWSI project because Santa Fe is interested in a much larger shaft than is being considered for the ES. Also, the ability to seal the Santa Fe casing concept, reinforced concrete sections, has not been demonstrated, and the risk and resulting consequences, should it fail, may be unacceptable.

IX. QUALITY ASSURANCE (P. L. Bussolini, R. R. Geoffrion, and J. J. Simpson)

A. Los Alamos National Laboratory

Sandia Quality Assurance (QA) Overview and WMPO/NV performed an audit of the NNWSI project, and Los Alamos QA performed an audit of the Matrix Diffusion Studies conducted at the University of Arizona.

A meeting was held with Richard Shaw, Los Alamos Technical Associates, to update him on Los Alamos QA efforts in the NNWSI project. He is under contract to Sandia National Laboratory for NNWSI QA work at that facility.

Surveillance of program activities was performed. This surveillance was documented on QA checklists.

B. US Geological Survey

A package of approved USGS quality assurance procedures was sent to Don Vieth, DOE/HQ. A QA meeting conducted by DOE/HQ in Washington, D.C. was attended by the QA Manager and the Associate Group Leader for Waste Management QA.

During the quarter, eleven procedures were approved. The procedures were distributed to holders of the USGS Manual of Procedures. A total of seven other technical detailed procedures and a Unit Task Procedure were also sent to Denver for approval during the quarter.

X. PUBLICATIONS AND ABSTRACTS

1. P. R. Carroll, F. A. Caporuscio, and D. L. Bish, "Further Description of the Petrology of the Topopah Springs Member of the Paintbrush Tuff in Drill Holes UE25a-1 and USW-G1, and of the Lithic-Rich Tuff in USW-G1, Yucca Mountain, Nevada," Los Alamos National Laboratory report LA-9000-MS (November 1981).

2. D. L. Bish, "Detailed Mineralogical Characterization of the Bullfrog and Tram Members in USW-G1, with Emphasis on Clay Mineralogy", Los Alamos National Laboratory report LA-9021-MS (October 1981).

3. B. Crowe, S. Self, and R. C. Amos, "Strombolian Eruptive Sequences," (abs.): EOS, Trans. Am. Geophys. Union 62, 1084 (1981).

4. R. C. Amos, S. Self, and B. Crowe, "Pyroclastic Activity of Sunset Crater: Evidence for a Large Magnitude, High Dispersal Stromoblian Eruption," (abs.): EOS, Trans. Am. Geophys. Union 62, 1085 (1981).

ACKNOWLEDGMENTS

The following Los Alamos National Laboratory personnel are acknowledged for the efforts mentioned: D. A. Mann (technical assistance), P. A. Elder, M. E. Lark, and S. Lermuseaux (sample counting and gamma-spectral analyses), and L. M. Mitchell and C. E. Gallegos (typing of drafts and final manuscript).

REFERENCES

1. B. R. Erdal, W. R. Daniels, D. T. Vaniman, and K. Wolfsberg, Eds., "Research and Development Related to the Nevada Nuclear Waste Storage Investigations, April 1 - June 30, 1981," Los Alamos National Laboratory report LA-8959-PR (October 1981).

2. B. R. Erdal, W. R. Daniels, and K. Wolfsberg, Eds., "Research and Development Related to the Nevada Nuclear Waste Storage Investigations, January 1 - March 31, 1981," Los Alamos National Laboratory report LA-8847-PR (July 1981).

3. I. Neretnieks, "Diffusion in the Rock Matrix - an Important Factor in Radionuclide Migration?" Kärnbränlesäkerhet report KBS-79-19 (May 1979).

4. A. Rasmuson and I. Neretnieks, "Migration of Radionuclides in Fissured Rock - The Influence of Micropore Diffusion and Longitudinal Dispersion," Kärnbränslesäkerhet report KBS-80-24 (December 1979).

5. I. Neretnieks, "Diffusion in the Rock Matrix - An Important Factor in Radionuclide Retardation?" J. Geophys. Res. 85, 4379 (1980).

6. K. Wolfsberg, R. D. Aguilar, B. P. Bayhurst, W. R. Daniels, S. J. DeVilliers, B. R. Erdal, F. O. Lawrence, S. Maestas, A. J. Mitchell, P. Q. Oliver, N. A. Raybold, R. S. Rundberg, J. L. Thompson, and E. N. Vine, "Sorption-Desorption Studies on Tuff. III. A Continuation of Studies with Samples from Jackass Flats and Yucca Mountain, Nevada," Los Alamos National Laboratory report LA-8747-MS (May 1981).

7. K. Wolfsberg, B. P. Bayhurst, B. M. Crowe, W. R. Daniels, B. R. Erdal, F. O. Lawrence, A. E. Norris, and J. R. Smyth, "Sorption-Desorption Studies on Tuff. I. Initial Studies with Samples from the J-13 Drill Site, Jackass Flats, Nevada," Los Alamos Scientific Laboratory report LA-7480-MS (April 1979).

8. E. N. Vine, R. D. Aguilar, B. P. Bayhurst, W. R. Daniels, S. J. DeVilliers, B. R. Erdal, F. O. Lawrence, S. Maestas, P. Q. Oliver, J. L. Thompson, and K. Wolfsberg, "Sorption-Desorption Studies on Tuff. II. A Continuation of Studies from Samples from Jackass Flats, Nevada, and Initial Studies with Samples from Yucca Mountain, Nevada," Los Alamos Scientific Laboratory report LA-8110-MS (January 1980).

9. W. R. Daniels, Ed., "Laboratory Studies of Radionuclde Distributions Between Selected Groundwaters and Geologic Media, October 1, 1979 - September 30, 1980," Los Alamos National Laboratory report LA-8586-PR (January 1981).

10. C. F. Baes and R. E. Mesmer, The Hydrolysis of Cations (John Wiley and Sons, New York, 1976), p. 190.

11. D. A. Buckingham, F. P. Dwyer, H. A. Goodwin, and A. M. Sargeson, "Mono- and Bis-(2,2´-Bipyridine) and (1,10-Phenanthroline) Chelates of Ruthenium and Osmium," Aust. J. Chem. 17, 325 (1964).

12. R. H. Fabian, D. M. Klassen, and R. W. Sonntag, "Synthesis and Spectroscopic Characterization of Ruthenium and Osmium Complexes with Sterically Hindering Ligands," Inorg. Chem. 19, 1977 (1980).

13. J. Boulègue, "Electrochemistry of Reduced Sulfur Species in Natural Waters - I. The H_2S - H_2O System," Geochim. Cosmochim. Acta 42, 1439-1445 (1978).

14. J. Boulègue and G. Michard, "Sulfur Speciations and Redox Processes in Reducing Environments," in Chemical Modeling in Aqueous Systems, E. Jenne, Ed. (American Chemical Society, Washington, D.C., 1979), p. 25.

15. S. L. Schoff and J. E. Moore, "Chemistry and Movement of Ground Water, Nevada Test Site," US Geol. Surv. report TEI-838 (1964).

16. G. E. Manger, "The Best Value of Porosity of Lapilli Tuff from the Nevada Test Site, US Geol. Surv. Prof. Paper 525-B (1965), pp. B146-B150.

17. R. A. Robinson and R. H. Stokes, Electrolyte Solutions (Butterworths, London, 1968), pp. 253-257.

18. P. Spacek and M. Kubin, "Diffusion in Gels," J. Polym. Sci. C 16, 705 (1967).

19. L. K. Porter, W. D. Kemper, R. D. Jackson, and B. C. Stewart, "Chloride Diffusion in Soils is Influenced by Moisture Content," Soil Sci. Soc. Am. Proc. 24, 460 (1960).

20. R. Kuhn and A. Wasserman, "Die Dissoziationskonstanten der Halogenbenzoesauren," Helv. Chim. Acta 11, 31 (1928).

21. M. T. Ryan and K. J. Berner, "Λ_{OH} and pKa Values of Para Substituted Tetrafluorobenzoic Acids," Spectrochim. Acta 25A, 1155 (1969).

22. W. J. Moore, Physical Chemistry (Prentice Hall, Englewood Cliffs, N.J., 1972), pp. 425-427.

23. G. I. Taylor, "Dispersion of Matter in Solvent Flowing Slowly Through a Tube," Proc. Roy. Soc. London A 219, 186 (1953).

24. T. J. Wolery and L. J. Walters, Jr., "Calculation of Equilibrium Distributions of Chemical Species in Aqueous Solutions by Means of Monotone Sequences", J. Int. Assoc. Math. Geol. 7, 99 (1975).

25. J. Crank, The Mathematics of Diffusion, 2nd ed. (Oxford University Press, London, 1975), p. 52.

26. J. B. Ball, D. K. Nordstrom, and E. A. Jenne, "Additional and Revised Thermochemical Data and Computer Code for WATEQ2 - A Computerized Chemical Model for Trace and Major Element Speciation and Mineral Equilibria of Natural Waters," US Geol. Surv. Water Resources Invest. report WRI 78-116 (January 1980).

27. T. J. Wolery, "Calculations of Chemical Equilibrium between Aqueous Solution and Minerals: The EQ3/6 Software Package," Lawrence Livermore Laboratory report UCRL-52658 (February 1979).

28. G. Sposito and S. V. Mattigod, "GEOCHEM: A Computer Program for the Calculation of Chemical Equilibria in Soil Solutions and Other Natural Water Systems," Department of Soil and Environmental Sciences, University of California, Riverside, California (1979).

29. S. E. Ingle, M. D. Schuldt, and D. W. Schults, "A User's Guide for REDEQL.EPAK," Environ. Prot. Agency report EPA-600/3-78-024 (February 1978).

30. S. E. Ingle, J. A. Keniston, and D. W. Shults, "REDEQL.EPAK, Aqueous Chemical Equilibrium Program," Corvallis Environmental Research Laboratory, Corvallis, Oregon (1979).

31. L. N. Plummer, B. F. Jones, and A. H. Truesdell, "WATEQF: A FORTRAN IV Version of WATEQ, A Computer Program for Calculating Chemical Equilibrium of Natural Waters, Users Guide," US Geol. Surv. report USGS-WRI-76-13 (September 1976).

32. D. L. Bish, "Detailed Mineralogical Characterization of the Bullfrog and Tram Members in USW-G1, with Emphasis on Clay Mineralogy", Los Alamos National Laboratory report LA-9021-MS (October 1981).

33. D. L. Bish, F. A. Caporuscio, J. F. Copp, B. M. Crowe, J. D. Purson, J. R. Smyth, and R. G. Warren, "Preliminary Stratigraphic and Petrologic Characterization of Core Samples from USW-G1, Yucca Mountain, Nevada," A. C. Walters and P. R. Carroll, Eds., Los Alamos National Laboratory report LA-8840-MS (November 1981).

34. J. Hoffman and J. Hower, "Clay Mineral Assemblages as Low Grade Metamorphic Geothermometers: Application to the Thrust Faulted Disturbed Belt of Montana, U.S.A.," in Aspects of Diagenesis, P. A. Scholle and P. R. Schluger, Eds., Soc. Econ. Paleontol. Mineral. Spec. Publ. 26, 55 (1979).

35. J. Srodon, "Precise Identification of Illite/Smectite Interstratifications by X-ray Powder Diffraction," Clays and Clay Miner. 28, 401 (1980).

36. R. C. Reynolds, Jr., "The Effect of Particle Size on Apparent Lattice Spacings," Acta Crystallogr. A24, 319 (1968).

37. H. E. Roberson and R. W. Lahann, "Smectite to Illite Conversion Rates: Effects of Solution Chemistry," Clays and Clay Miner. 29, 129 (1981).

38. E. A. Perry and J. Homer, "Burial Diagenesis of Gulf Coast Pelitic Sediments," Clays and Clay Miner. 18, 165 (1970).

39. B. M. Crowe and W. J. Carr, "Preliminary Assessment of the Risk of Volcanisn at a Proposed Nuclear Waste Repository in the Southern Great Basin," US Geol. Surv. Open File report 80-357 (1980).

40. B. Crowe, S. Self, and R. C. Amos, "Strombolian Eruptive Sequences," (abs.): EOS, Trans. Am. Geophys. Union 62, 1084 (1981).

☆U.S. GOVERNMENT PRINTING OFFICE: 1982-0-576-020/11